Universidad de Concepción
Dirección de Postgrado
Facultad de Ingeniería – Programa de Magíster en Ciencias de la Ingeniería con Mención en Ingeniería Civil

Assessment of the seismic performance of a RC building designed following two alternative approaches: NCh433+DS61 versus ACHISINA PBEE requirements

POR PAULO JAVIER TORRES OSORIO

Tesis presentada a la Facultad de Ingeniería de la Universidad de Concepción para optar al grado de Magíster en Ciencias de la Ingeniería con mención en Ingeniería Civil

Profesor Guía: Dr. Pablo Parra Torres
Profesor Co-Guía: Dr. Patricio Cendoya Hernández

Septiembre, 2023
Concepción, Chile

Se autoriza la reproducción total o parcial, con fines académicos, por cualquier medio o procedimiento, incluyendo la cita bibliográfica del documento.

ACKNOWLEDGEMENTS

I want to thank M.Sc. Francisco Acuña for his help with the geotechnical characterization of the building site; Ph.D. candidate Marco Gallegos for his support with the scripts to obtain results from PERFORM-3D binary files, which was fundamental to getting the results presented in the last chapters; and Felipe Solís for sharing his knowledge of non-linear dynamic analysis software.

I also want to thank the SIBER-RISK Strong Motion Database team for sharing their Chilean record database used for the studies in this thesis.

Lastly, I want to thank Dr. Pablo Parra and Dr. Patricio Cendoya for their continuous support and knowledge sharing in developing this thesis.

INDEX OF CONTENTS

CHAPTER 1 INTRODUCTION 1

1.1 Motivation 1

1.2 Hypothesis 2

1.3 Objectives 2

1.3.1 General Objective 2

1.3.2 Specific Objectives 2

1.4 Methodology 2

1.5 Contents of this report 3

CHAPTER 2 CALIBRATION AND VALIDATION OF PARAMETERS FOR NONLINEAR MODELING 4

2.1 Introduction 4

2.2 Experimental tests 4

2.3 Numerical models 6

2.4 Conclusions 14

CHAPTER 3 CODE-BASED ANALYSIS AND DESIGN OF STUDY BUILDING 15

3.1 Introduction 15

3.2 Building description 15

3.3 ETABS model 16

3.4 Seismic response 19

3.5 Design of slender walls 21

3.6 Conclusions 26

CHAPTER 4 NONLINEAR MODELING OF STUDIED BUILDING 27

4.1 Introduction 27

4.2 Structural modeling 27

4.3 ACHISINA PBEE requirements 31
4.4 Conclusion 34
CHAPTER 5 EVALUATION OF ACHISINA PBEE REQUIREMENTS 35
5.1 Introduction 35
5.2 Modal pushover analysis results 35
5.3 Dynamic analysis results 36
5.4 Evaluation of alternative modeling approaches 40
5.5 Comparison between ACHISINA and LATBSDC requirements 48
5.6 Conclusion 52
CHAPTER 6 CONCLUSIONS AND CLOSING REMARKS 53
BIBLIOGRAPHY 55
APPENDIX A CONCRETE CONSTITUTIVE CURVES 58
A1 Confined concrete strength 58
A2 Stress-strain relationship 60
APPENDIX B SEISMIC HAZARD ANALYSIS RESULTS 62

INDEX OF TABLES

Table 2.1. Concrete compression stress-strain parameters (Lowes *et al.*, 2016). 9
Table 2.2. Concrete cyclic energy factors (Lowes *et al.*, 2016). 10
Table 3.1. Applied dead and live loads per story in the ETABS model. 17
Table 3.2. Load combinations used in the ETABS model. 19
Table 3.3. Results for the earthquake in the X direction. 20
Table 3.4. Results for the earthquake in the Y direction. 20
Table 3.5. Horizontal displacement verifications in each principal direction. 21
Table 3.6. Designed reinforcement at boundary elements. 24
Table 4.1. Values for each limit state in reinforced concrete walls (ACHISINA, 2017). 32
Table 4.2. Selected records from the SIBER-RISK (2020) database. 34
Table 5.1. Fundamental periods for different models. 35
Table 5.2. Maximum shear values obtained for all SD earthquakes per wall group. 39
Table 5.3. Maximum shear values obtained for all matched SD earthquakes per wall group. 43
Table 5.4. Maximum shear values obtained for all SMC earthquakes per wall group. 43
Table 5.5. Maximum shear values obtained for all SD earthquakes per wall group. 47
Table 5.6. Maximum shear values obtained for all SMC earthquakes per wall group. 47
Table 5.7. Maximum shear values obtained for the SLE earthquakes per wall group. 52
Table B.1. Weighting for the different attenuations for the PSHA. 62
Table B.2. Hazard curve results (Atkinson and Boore). 63
Table B.3. Hazard curve results (Zhao *et al.*). 65
Table B.4. Hazard curve results (Montalva *et al.*). 67
Table B.5. Hazard curve results (BC Hydro). 69
Table B.6. Hazard curve results (Youngs *et al.*). 71
Table B.7. Hazard curve results (weighted average). 73

INDEX OF FIGURES

Fig. 2.1. RW2 wall cross-section and reinforcement (after Thomsen and Wallace, 1995).... 4
Fig. 2.2. TW2 wall cross-section and reinforcement (after Thomsen and Wallace, 1995).... 5
Fig. 2.3. Testing instrumentation of rectangular walls (after Thomsen and Wallace, 1995). 5
Fig. 2.4. Displacement history for RW2 and TW2 walls (after Thomsen and Wallace, 1995). 6
Fig. 2.5. Typical YULRX envelope for materials (after CSI, 2016). 8
Fig. 2.6. Concrete (unconfined and confined) and steel YULRX envelopes (1 ksi = 6.89 MPa, 1 in. = 0.0254 m) 8
Fig. 2.7. Meshes and loads for (a) RW2 wall specimen and (b) TW2 wall specimen. 11
Fig. 2.8. Lateral load versus deformation history for RW2 wall (1 kip = 4.45 kN). 12
Fig. 2.9. Lateral load versus deformation history for TW2 wall (1 kip = 4.45 kN). 12
Fig. 2.10. Wall strain gradient for wall RW2. 13
Fig. 2.11. Wall strain gradient for wall TW2, flange in compression. 13
Fig. 2.12. Wall strain gradient for wall TW2, flange in tension. 14
Fig. 3.1. Plan view of the study building, after Cando *et al*.(2020). 15
Fig. 3.2. Building model in commercial software ETABS. 16
Fig. 3.3. NCh433+DS61 design spectrum. 18
Fig. 3.4. Story shears in the X direction (blue) and Y direction (orange). 20
Fig. 3.5. Moment-curvature diagram for wall 1 in SAP2000. 22
Fig. 3.6. Strain diagram for wall 1 for ε_c = 0.008. 23
Fig. 3.7. Boundary elements in each direction for T-shaped walls: (a) 0° rotation; (b) 180° rotation; (c) 90° rotation; (d) 270° rotation. 24
Fig. 3.8. Boundary elements for Walls 1 and 3, respectively. 25
Fig. 3.9. Boundary element for Wall 2 flange. 25
Fig. 3.10. Boundary element for Wall 2 flange. 25
Fig. 3.11. Boundary element for Wall 2 web. 26
Fig. 4.1. Proposed stress-strain relationship for Wall 1 (1 kN/m^2 = 0.001 MPa). 27
Fig. 4.2. Proposed YULRX concrete curves for the first four stories of all walls (1 kN/m^2 = 0.001 MPa). 28
Fig. 4.3. Proposed YULRX steel curves for all walls (1 kN/m^2 = 0.001 MPa). 28

Fig. 4.4. Shear material constitutive curve for all walls (1 kN/m^2 = 0.001 MPa). 29
Fig. 4.5. Elements defined in the PERFORM-3D model. 30
Fig. 4.6. Earthquake record selection flowchart. 33
Fig. 4.7. SRSS-combined mean of the displacement spectra for the chosen earthquakes. .. 34
Fig. 5.1. Pushover curves in the study building's longitudinal direction (H_1) and the transverse direction (H_2). 36
Fig. 5.2. Flowchart for Deformation Gage element results through PERFORM-3D binary files. 37
Fig. 5.3. Strain profiles for Walls 1, 2, 3, and 4 for the SD group versus ACHISINA limits, respectively. 38
Fig. 5.4. Maximum story drifts at each story level versus ACHISINA limits. 39
Fig. 5.5. Response spectra for the original earthquakes in each direction. 40
Fig. 5.6. Response spectra for the matched earthquakes in each direction. 41
Fig. 5.7. SRSS-combined mean of the spectra for the matched earthquakes. 41
Fig. 5.8. Strain profiles for Walls 1, 2, 3, and 4 for the SD-matched records. 42
Fig. 5.9. Strain profiles for Walls 1, 2, 3, and 4 for the amplified matched records (SMC). 43
Fig. 5.10. Maximum story drifts at each story level for the matched SD records. 44
Fig. 5.11. Finite element for the slab elements for the second iteration of the model. 45
Fig. 5.12. SD strain profiles for Walls 1, 2, 3, and 4 for the model with elastic slabs. 45
Fig. 5.13. SMC strain profiles for Walls 1, 2, 3, and 4 for the model with elastic slabs. 46
Fig. 5.14. Strains over time for records 1 to 4 in (a) gage element 625, and (b) gage element 649 (both at the base of wall 4). 47
Fig. 5.15. Maximum story drifts at each story level for the model with slabs. 48
Fig. 5.16. Comparison between UHS for three different return periods and the code-based SD and SMC spectra. 50
Fig. 5.17. Response spectra for the matched SLE earthquakes for nonlinear analysis. 51
Fig. 5.18. SLE strain profiles for Walls 1, 2, 3, and 4 for the model with elastic slabs. 51
Fig. 5.19. Maximum story drifts for the SLE at each story level. 52
Fig. A.1. Wall 1 boundary element. 59
Fig. A.2. Proposed stress-strain relationship (adapted from Saatcioglu and Razvi, 1992). . 60
Fig. A.3. Proposed stress-strain relationship for Wall 1. 61

ABSTRACT

Chile is one of the world's most seismically active countries, with two earthquakes on the list of the ten largest earthquakes ever recorded (M_w 9.5 Valdivia, 1960; M_w 8.8 Maule, 2010). The seismic design of buildings in Chile follows the NCh433 standard, based on a traditional approach that uses reduced earthquake forces applied over linear elastic models. Following the 2010 Chile earthquake, two supreme decrees were published (DS60 and DS61), which modified some NCh433 requirements concerning the design of reinforced concrete (RC) buildings. In 2017, the Chilean Association of Seismology and Earthquake Engineering (ACHISINA) introduced an alternative performance-based (PBEE) procedure to design RC buildings. This document is based on the proposals of the Los Angeles Tall Building Structural Design Council (LATBSDC). The ACHISINA document clearly defined several earthquake levels, performance objectives, and limit states to understand better the behavior of buildings subjected to these ground motions, opening a window to obtain alternative designs which hopefully can reduce involved costs. In this study, a 20-story tall RC shear wall building, considered a typical Chilean residential building, was designed following the NCh433+DS61 requirements. Later, nonlinear analyses were conducted to verify if this building satisfied the requirements of the ACHISINA PBEE document and explore if it is possible to reduce the project costs by introducing design changes. Three different modeling techniques for the whole building were evaluated. Analyses showed that the building did not satisfy the story drift limits established in the ACHISINA PBEE document; therefore, design changes are impossible. Later, this thesis compares the requirements of the ACHISINA PBEE document and the LATBSDC PBEE document, discussing the changes introduced in the Chilean document and the impact on actual designs.

CHAPTER 1 INTRODUCTION

1.1 Motivation

The M_w 8.8 Maule earthquake in 2010 made possible the study of the seismic performance of residential buildings. These structures typically use RC walls as the primary gravity and seismic force-resisting system, with a wall plan density of approximately 3% in each principal direction. It was observed that only 2% of the buildings reached a significant level of damage (Massone *et al.*, 2012). As a consequence of the reported damage following the 2010 earthquake, in 2011, two supreme decrees were published, DS60 (MINVU, 2011a) and DS61(MINVU, 2011b), adding new requirements to the seismic design standard NCh433 (INN, 2012) regarding wall confinement and seismic demands considered for analysis and design. Although NCh433 declares performance objectives to limit damage under frequent earthquakes and avoid collapses during exceptionally severe earthquakes, it does not clearly define a frequent or powerful earthquake and how to measure these performance objectives.

In 2017, the Asociación Chilena de Sismología e Ingeniería Antisísmica (ACHISINA) published its performance-based design (PBEE) document (ACHISINA, 2017), explicitly defining a design and a maximum earthquake with their respective limit states and performance levels, based on the Los Angeles Tall Buildings Structural Design Council proposal (LATBSDC, 2015). Currently, a new version of NCh433 is under public consultation. This version allows using performance-based engineering as a valid alternative for the structural design of tall buildings in Chile.

The ACHISINA document establishes that the proposed PBEE design leads to safer buildings than the actual NCh433 requirements. However, there is little to no information about the application of this methodology in Chilean buildings, in addition to costs, damage, and economic losses associated with this design method. Thus, studying the advantages and disadvantages of this alternative design methodology is mandatory.

In this research project, the ACHISINA PBEE requirements are used to evaluate a 20-story shear wall building designed under the standard NCh433+DS61 requirements, to evaluate design changes to reduce project costs.

1.2 Hypothesis

A 20-story shear wall building designed following NCh433+DS61 meets the ACHISINA PBEE requirements. Design modifications can be introduced to the building to reduce the project cost while still meeting the ACHISINA PBEE requirements.

1.3 Objectives

1.3.1 General Objective

To evaluate the seismic performance of a 20-story shear wall building designed following NCh433+DS61 using the alternative PBEE procedure published by ACHISINA in 2017.

1.3.2 Specific Objectives

- Determine the linear and nonlinear response of a Chilean habitational building to different seismic demands.
- Identify the advantages and disadvantages of different nonlinear modeling techniques for RC buildings.
- Assess the pertinence of using the ACHISINA PBEE document as an alternative procedure for designing RC shear wall buildings.

1.4 Methodology

This research project will design a typical Chilean habitational building following the NCh433+DS61 standards, which is a traditional force-based design method using linear spectral analysis. Then, this building will be subjected to nonlinear response history analysis

using the commercial software PERFORM-3D (CSI, 2016), following the alternative performance-based procedure defined by ACHISINA (2017). Validation and calibration of nonlinear parameters for RC shear walls are worked on first, following recommendations found in the literature (Lowes et al., 2016). Then, an alternative design will be proposed if the building satisfies the ACHISINA requirements focusing on reducing the economic costs.

The location defined for the building was the El Venado sector in San Pedro de la Paz, Biobío, Chile, defined as seismic zone 3 based on NCh433, with a soil V_{s30} of 409 m/s (FUCHIGE, 2014), classifying as a type C soil.

1.5 Contents of this report

Chapter 2 presents the calibration and validation of modeling parameters for nonlinear analysis using results of previous experimental programs conducted on isolated wall specimens (Thomsen & Wallace, 1995).

Chapter 3 documents the code-based analysis and design of the 20-story shear wall building.

Chapter 4 presents the nonlinear modeling of the studied building, including the definition of the performance objectives and ground motions.

Chapter 5 corresponds to the PBEE verification following the ACHISINA PBEE requirements (ACHISINA, 2017).

Chapter 6 presents the conclusions of the research project.

CHAPTER 2 CALIBRATION AND VALIDATION OF PARAMETERS FOR NONLINEAR MODELING

2.1 Introduction

In this chapter, parameters for nonlinear modeling are calibrated and validated by comparing the results from experimental tests with the corresponding computational models.

2.2 Experimental tests

Thomsen & Wallace (1995) performed cyclic tests on rectangular and T-shaped reinforced concrete wall specimens, tagged as RW2 and TW2, respectively. Both walls were 144 in. tall. Fig. 2.1 and Fig. 2.2 depict the reinforcing details. Longitudinal and transverse reinforcement considered Typical Grade 60 steel, while mean concrete compressive strengths at the base of each wall were 6.33 ksi for RW2 and 6.05 ksi for TW2.

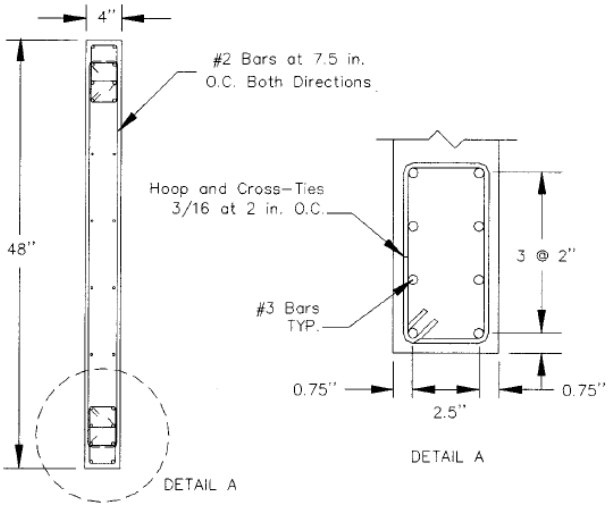

Fig. 2.1. RW2 wall cross-section and reinforcement (after Thomsen and Wallace, 1995)

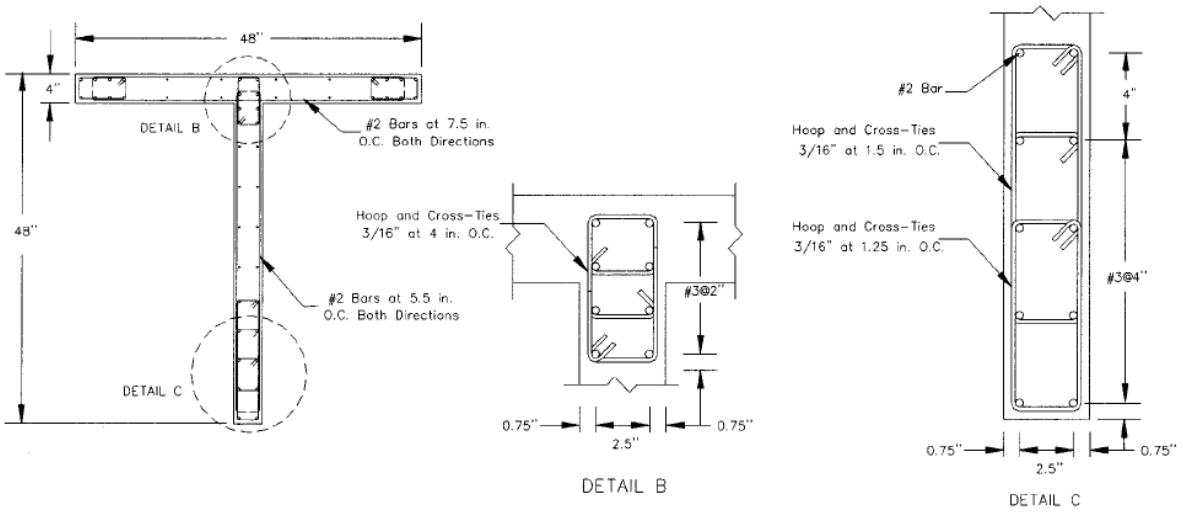

Fig. 2.2. TW2 wall cross-section and reinforcement (after Thomsen and Wallace, 1995).

Fig. 2.3 shows the setup used for testing the walls. During the test, hydraulic jacks applied constant axial loads of $0.10f'_cA_g$ at the top of both walls. Next, a hydraulic actuator applied lateral displacements, with drift cycles from 0.1% to 3.0%. Fig. 2.4 shows the lateral displacement history for each wall.

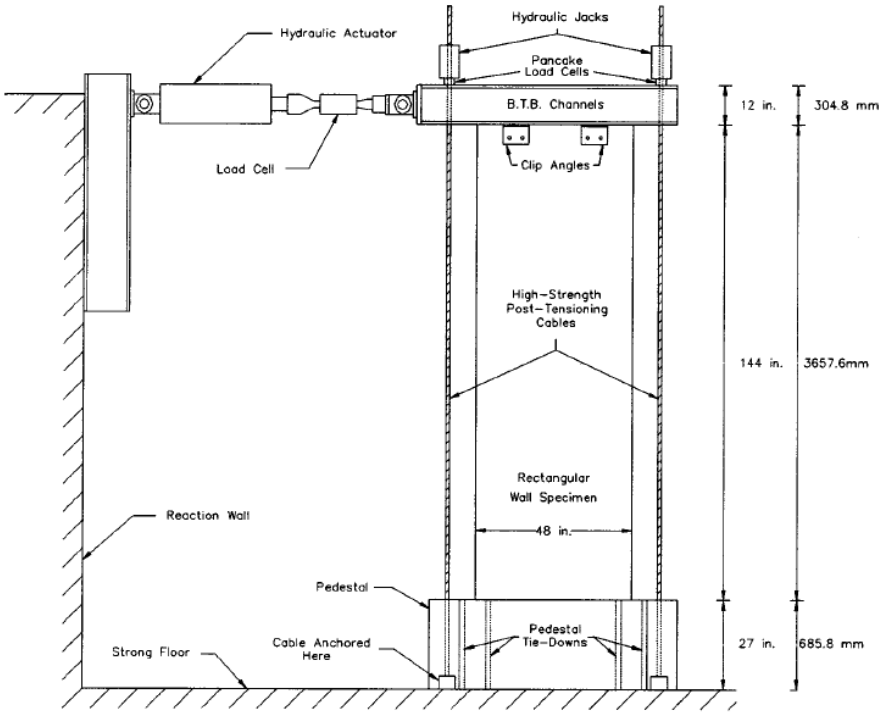

Fig. 2.3. Testing instrumentation of rectangular walls (after Thomsen and Wallace, 1995).

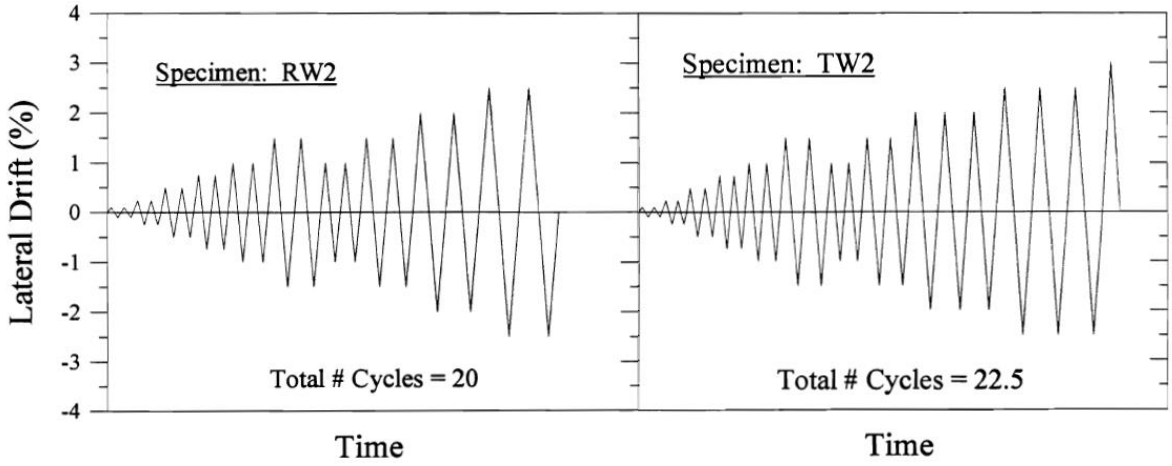

Fig. 2.4. Displacement history for RW2 and TW2 walls (after Thomsen and Wallace, 1995).

Also, wire potentiometers and LVDTs were used for measuring displacements, deformations, and loads at several locations on each wall. Concrete axial strains were measured using seven embedded concrete strain gauges for the rectangular wall and five for the T-shaped wall, all located approximately 2 inches above the pedestal-wall interface.

Results for specimen RW2 indicated that the wall maintained lateral capacity even after the two 2.5% drift cycles, attributed to the detailing of the transverse reinforcement at the wall boundaries. As for TW2, the wall maintained lateral capacity until the second and third 2.5% drift cycles, limited by out-of-plane buckling in the web boundary zone. As per lateral loads and concrete strain distributions for different drift levels, the following sections present the results.

2.3 Numerical models

PERFORM-3D (CSI, 2016) was used as an analysis platform for nonlinear modeling. The nonlinear analysis consists of two phases: modeling and analysis. The modeling phase details nodes, materials, elements, loads, and limit states, and the analysis phase defines load cases and combinations, runs nonlinear analyses, and shows several results, such as modal analysis results, deflected shapes, time histories, and others.

For reinforced concrete shear walls, two elements are available in the software: General Wall and Shear Wall elements. Both consist of 4-noded finite elements, with layers that account for vertical axial-bending interaction and horizontal shear. The General Wall element has a layer for horizontal axial bending and two layers for diagonal compression used to model strut and tie action, which makes this element harder to calibrate and more computationally demanding than the Shear Wall element.

In the Shear Wall element, longitudinal in-plane behavior is more critical and can be inelastic in bending and shear, while transverse and out-of-plane bending is secondary, and both are assumed to be elastic. This element's bending-axial behavior is modeled by cross sections with concrete and steel fibers, up to a maximum of 16 total fibers. The latter can be defined as a percentage of the concrete area using the Auto Size cross-section or by inputting the coordinates and areas of each fiber using the Fixed Size cross-section. The shear behavior is modeled by defining a shear material. This way, the wall can mesh horizontally into several Shear Wall elements, each with its respective cross sections.

For the RW2 and TW2 walls, the horizontal mesh consisted of two boundary elements and two elements in the web, modeled with the Fixed and Auto Size cross sections, respectively. Following recommendations from the literature (Lowes *et al.*, 2016), vertical meshing consisted of three elements in the first story, where a nonlinear response is expected, and one element per story for the other levels. As per the materials, curves for unconfined concrete, confined concrete, and steel were modeled following a YULRX envelope (stepwise linear), defined by five points: the first yielding point (Y), the ultimate strength point (U), the ductile limit point (L), the residual strength point (R), and the point where the deformation is so large that there is no point in continuing the analysis (X). Fig. 2.5 shows a typical YULRX curve.

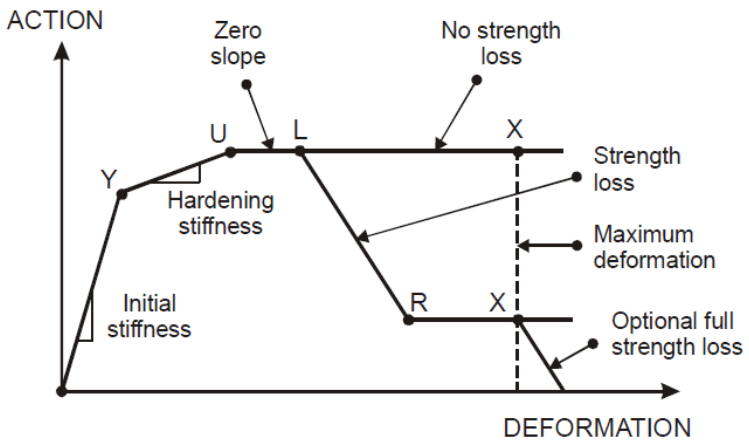

Fig. 2.5. Typical YULRX envelope for materials (after CSI, 2016).

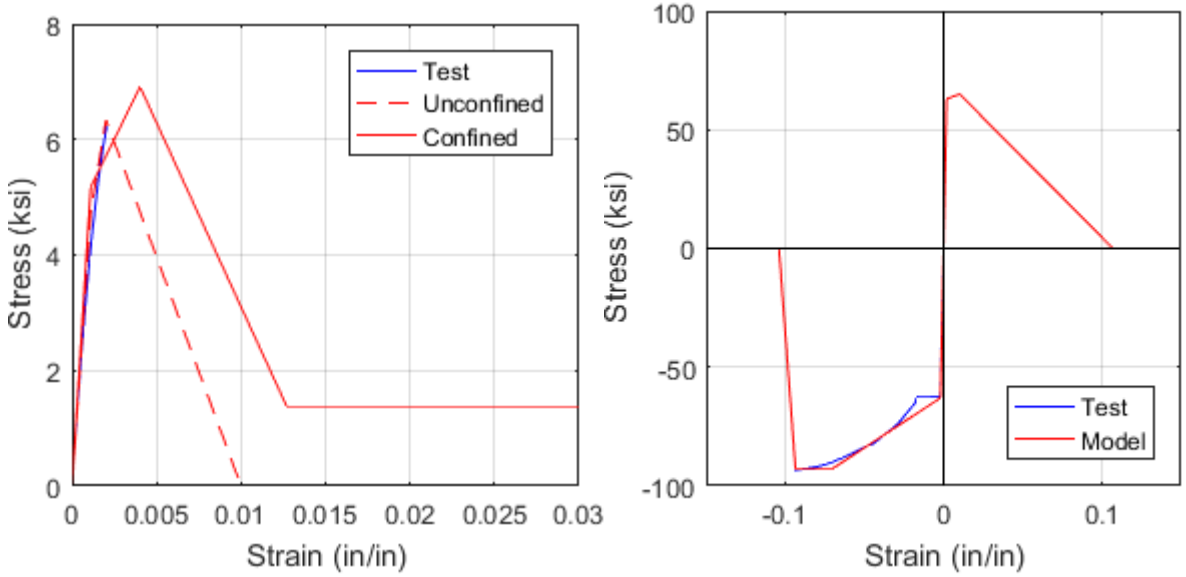

Fig. 2.6. Concrete (unconfined and confined) and steel YULRX envelopes (1 ksi = 6.89 MPa, 1 in. = 0.0254 m)

Fig. 2.6 shows the stress-strain curves for steel and concrete. Concrete elastic modulus was considered as $57000\sqrt{f_c'}$ psi, with f_c' in psi units (ACI, 2014). Several recommendations for modeling the materials were used (Lowes *et al.*, 2016). For concrete, strain-stress parameters from Table 2.1 were used, where $\varepsilon_{c,max}$ is defined by (Paulay and Priestley, 1992)

$$\varepsilon_{c,max} = 0.004 + 1.4\,\rho_h\,f_{yh}\varepsilon_{hm}/f'_{cc} \qquad \text{Eq. 2-1}$$

where ρ_h is the volumetric ratio of confining steel, f_{yh} and ε_{hm} are the yield strength and strain at the maximum strength of the confining reinforcement, and f'_{cc} is the confined concrete strength defined by Mander *et al.* (1988). Shear stiffness was defined as $0.1G_cA_g$ (PEER, 2014), where $G_c = 0.4E_c$, and A_g is the gross area of the wall.

	FY	**FU**	**FR/FU**	**DU (in./in.)**	**DL (in./in.)**	**DR (in./in.)**
Unconfined	0.75 f'_c	f'_c	0.001	0.002	0.00202	0.01
Confined	0.75 f'_{cc}	f'_{cc}	0.200	0.004	0.00404	$\varepsilon_{c,max}$

Table 2.1. Concrete compression stress-strain parameters (Lowes *et al.*, 2016).

Material regularization of the constitutive law for concrete and steel was applied to get mesh-independent results. The concrete material was regularized based on constant compressive fracture energy concepts, considering the fracture energy value G_{fc}= 0.5 kip/in. for unconfined concrete, and G_{fcc} (Eq. 2-2) for confined concrete.

$$0.5 < G_{fcc} = 2.5\left(\frac{f'_{cc}}{f'_c} - 0.85\right) < 1.25 \qquad \text{Eq. 2-2}$$

Eq. 2-3 and Eq. 2-4 present the strain at residual strength DR for unconfined and confined concrete, respectively

$$\varepsilon_R = DR = \varepsilon_o - \frac{f'_c}{E_c} + 2\frac{\left(\frac{G_{fc}}{L_{elem}}\right)}{f'_c} \qquad \text{Eq. 2-3}$$

$$\varepsilon_{Rcc} = DR_{cc} = \varepsilon_{occ} - \frac{f'_{cc}}{E_{cc}} + \frac{5}{3}\frac{\left(\frac{G_{fcc}}{L_{elem}}\right)}{f'_c} \qquad \text{Eq. 2-4}$$

where ε_o is the compressive strain at maximum concrete strength, f'_c is the concrete compressive strength, E_c is the concrete elastic modulus, G_{fc} is the concrete crushing energy and L_{elem} is the wall element height. Eq. 2-4 contains a *cc* subscript to account for the same listed properties but for confined concrete.

Based on the tested stress-strain relationship, steel was modeled with a non-buckling material. Regularization of the steel material consisted of a simplified buckling model

proposed by Pugh *et al.* (2015), which assumes that steel loses compressive capacity when the concrete reaches residual strength.

Additionally, cyclic response parameters were calibrated to account for stiffness loss, namely, the energy dissipation factor for both materials and the stiffness factor for steel. The energy dissipation factor is equal to the ratio of energy dissipated in a stress-strain cycle for the material with stiffness loss to the energy dissipated without stiffness loss and varies from 0 to 1. The stiffness factor determines whether the unloading, reloading stiffness, or both are reduced and varies from -1 to +1. Steel energy dissipation and stiffness factors were considered equal to 0.75 and 0.5, respectively. Table 2.2 shows concrete energy dissipation factors for each material state.

Material state	**Y (yield)**	**U (ultimate)**	**L (loss)**	**R (residual)**	**X (rupture)**
Energy factor	1.0	0.4	0.4	0.1	0.1

Table 2.2. Concrete cyclic energy factors (Lowes *et al.*, 2016).

After defining the steel and concrete materials, cross sections and Shear Wall compounds were determined and assigned to each element based on the cross sections given in Fig. 2.2. Each boundary element consisted of three up to four concrete fibers and two steel fibers, defined with the Fixed Size option, and web elements consisted of eight concrete fibers and four up to eight steel fibers, specified with the Auto Size option. Strain gage elements were also located between wall elements where an inelastic response was expected. Once the mesh and elements were assigned, loads were applied to the model in the *Load Patterns* menu. Axial loads were uniformly applied through the length of the wall, and lateral displacements were applied later as pushover load cases. Fig. 2.7 shows the meshes and direction of loads for each wall.

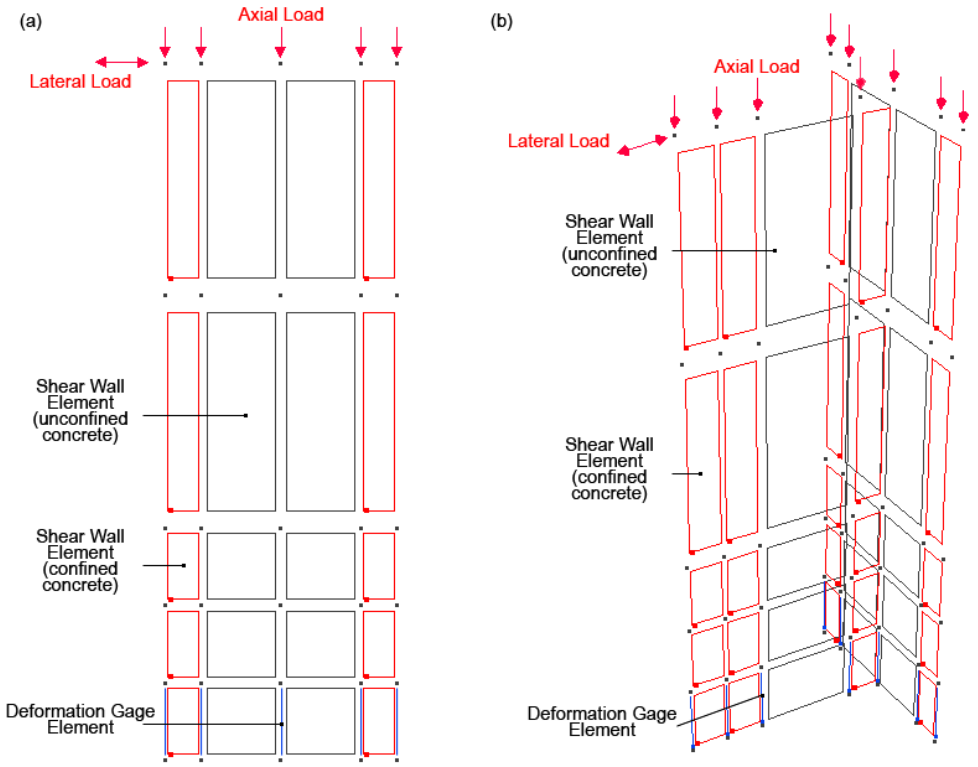

Fig. 2.7. Meshes and loads for (a) RW2 wall specimen and (b) TW2 wall specimen.

Fig. 2.8 and Fig. 2.9 show the lateral load versus lateral drift results for walls RW2 and TW2, respectively. Generally, the global response is well predicted but slightly overestimated for RW2 and TW2 with flange in compression by 5.2% and 8.6% versus the test results, respectively. When the flange is in tension in the T-shaped wall, the peak strength exceeds the experimental results by 32%. Several results show that PERFORM-3D models tend to overestimate these values (NEHRP, 2010; Ugalde et al., 2019). The global response of the wall was considered accurate enough for this study.

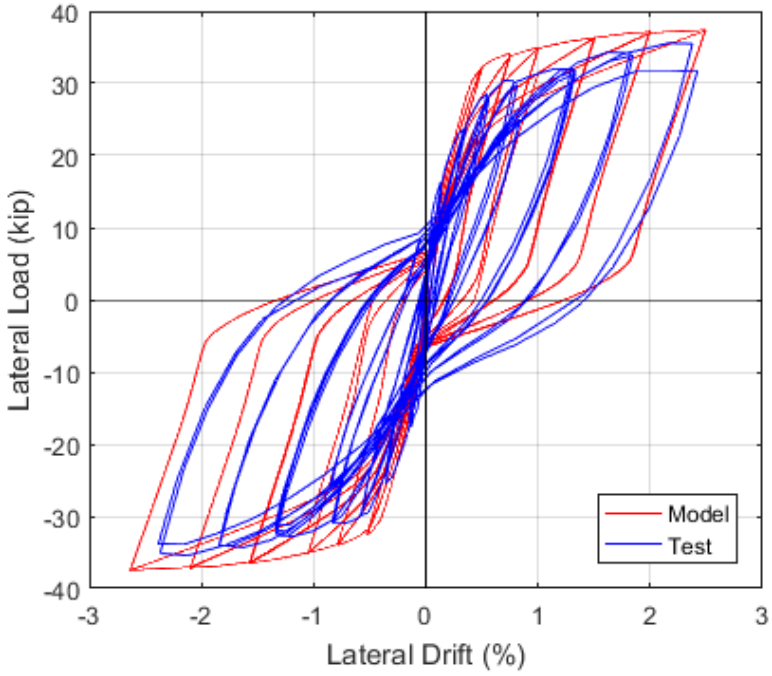

Fig. 2.8. Lateral load versus deformation history for RW2 wall (1 kip = 4.45 kN).

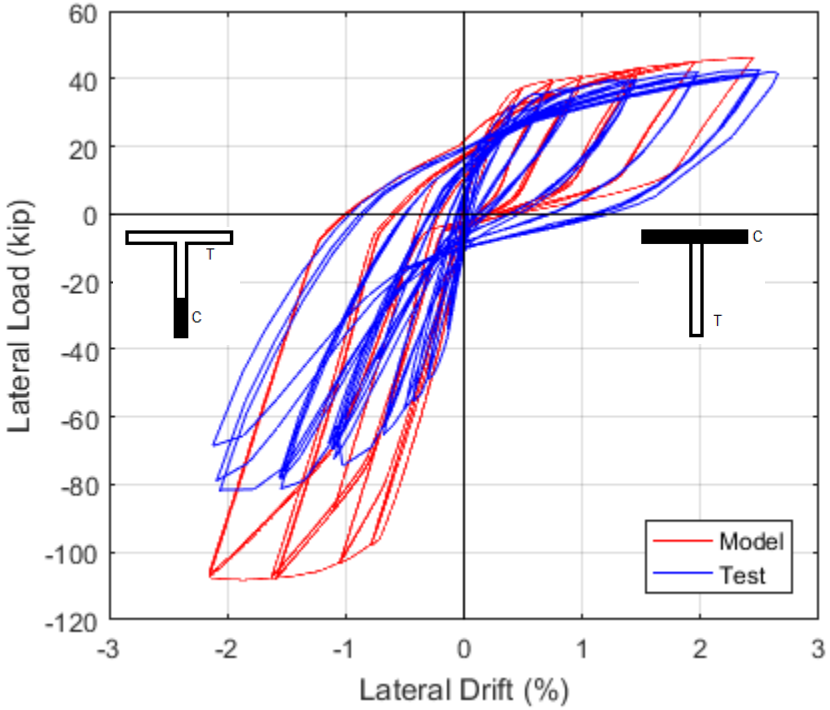

Fig. 2.9. Lateral load versus deformation history for TW2 wall (1 kip = 4.45 kN).

Fig. 2.10, Fig. 2.11, and Fig. 2.12 present the strain gradients at the wall base from each modeled wall.

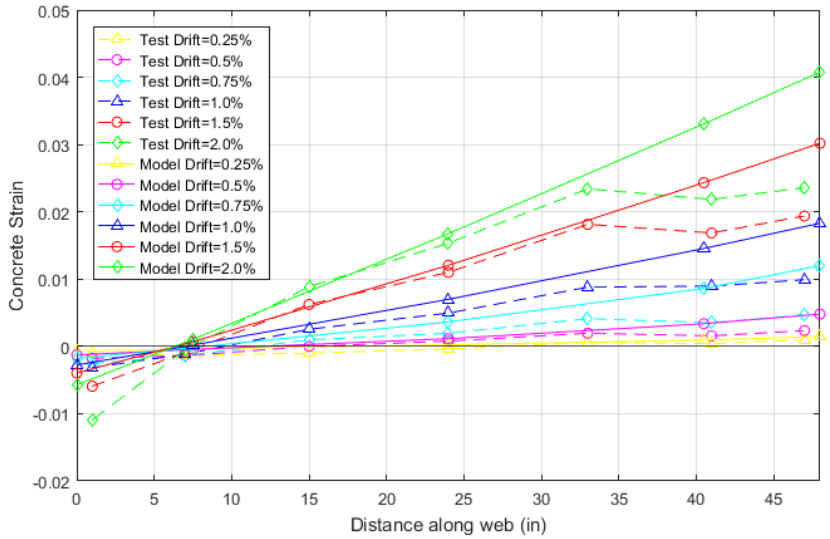

Fig. 2.10. Wall strain gradient for wall RW2.

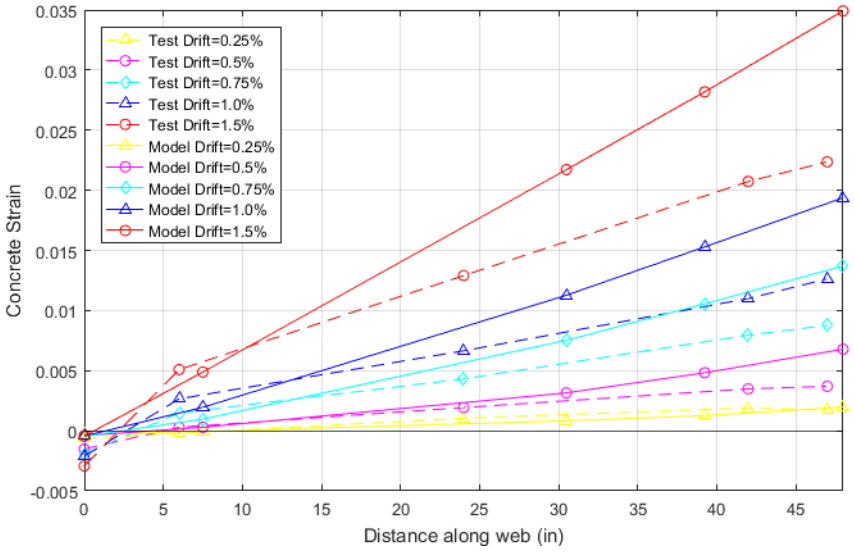

Fig. 2.11. Wall strain gradient for wall TW2, flange in compression.

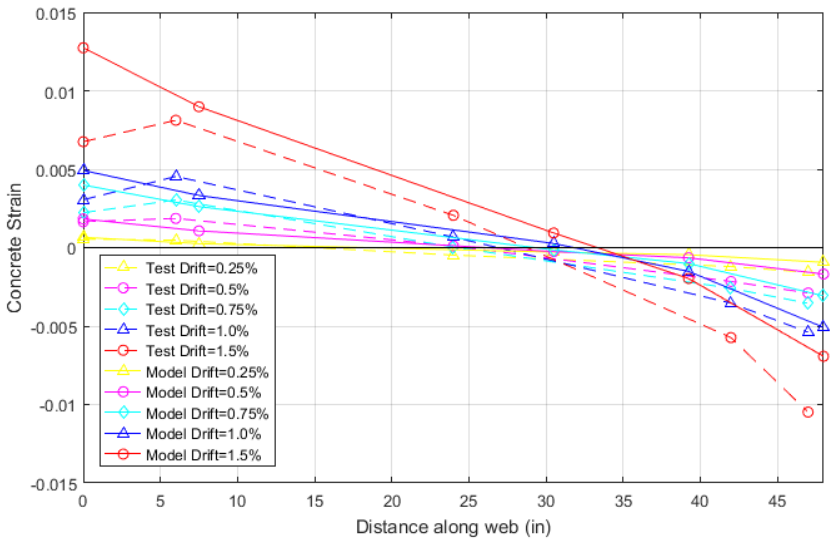

Fig. 2.12. Wall strain gradient for wall TW2, flange in tension.

These gradients show that local response quantities present more significant differences than global ones, which could be related to the Deformation Gage element in the model, which assumes constant strains between the end nodes of the gage, *i.e.*, from the base of the wall to a third of the first story height, while the actual strain gages in the walls have much shorter spans.

2.4 Conclusions

The PERFORM-3D model of both walls can accurately predict the global response quantities, as shown in Fig. 2.8 and Fig. 2.9, and can approximate the local response quantities near the center of the web, as shown in Fig. 2.10 to Fig. 2.12. Furthermore, these models were calibrated by following several recommendations from the literature, such as the definition of cyclic response parameters for each material, regularization of the concrete stress-strain curve by using the concrete crushing energy, and a simplified model to account for steel buckling.

CHAPTER 3 CODE-BASED ANALYSIS AND DESIGN OF STUDY BUILDING

3.1 Introduction

This chapter details the code-based analysis and design of the 20-story shear wall building studied in this research.

3.2 Building description

A 20-story shear wall building was designed following the NCh433 (INN, 2012) requirements, including supreme decrees DS60 (MINVU, 2011a) and DS61 (MINVU, 2011b). Fig. 3.1 depicts the building plan view obtained from Cando *et al.* (2020). The transverse wall density equals 4.2%, and the longitudinal wall density equals 2.8%. The typical story height is 2.6 m, the wall thickness is 300 mm, and the slab thickness is 160 mm.

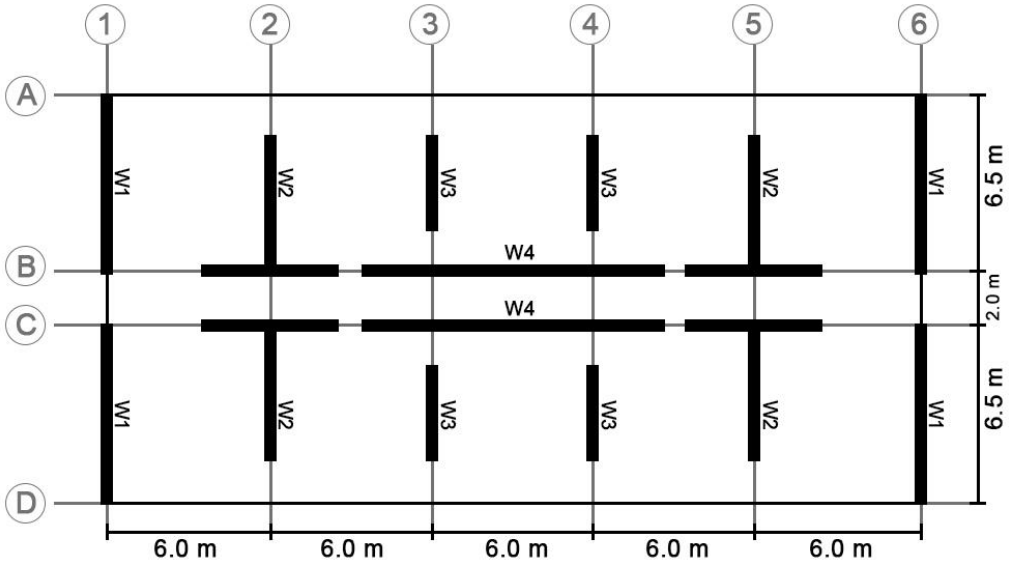

Fig. 3.1. Plan view of the study building, after Cando *et al.*(2020).

3.3 ETABS model

A 3D fixed-base linear-elastic model was developed in the commercial software ETABS (CSI, 2016a). Fig. 3.2 presents an isometric view of the computer model.

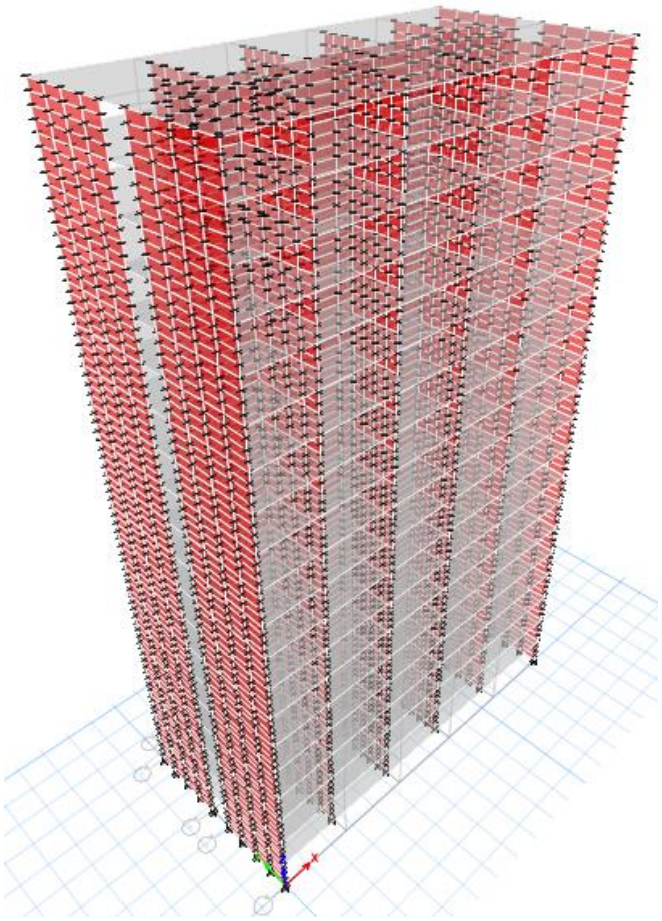

Fig. 3.2. Building model in commercial software ETABS.

Concrete and steel mechanical properties were defined as f_c' = 25 MPa and f_y = 420 MPa. Eq. 3-1 and Eq. 3-2 give the concrete elastic modulus (ACI, 2014) and the shear modulus, respectively

$$E_c = 4700\sqrt{f_c'} \text{ (MPa)} \quad \text{Eq. 3-1}$$

$$G_c = \frac{E_c}{2(1+\nu)} \quad \text{Eq. 3-2}$$

where ν = 0.2 is the Poisson's ratio for concrete.

The analysis and design considered three different load cases: dead load (DL), live load (LL), and seismic load (EQ). The first two were defined as uniform loads on slabs following the NCh1537 (INN, 2009) procedure without considering reduced loads for simplicity.

Story	DL (kgf/m^2)	LL (kgf/m^2)
20	385	100
1-19	670	200

Table 3.1. Applied dead and live loads per story in the ETABS model.

Seismic loads were calculated from the NCh433 (INN, 2012) design spectrum procedure, using Eq. 3-3 to obtain spectral accelerations

$$S_a = \frac{S\,A_0\,\alpha}{R^*/I} \qquad \text{Eq. 3-3}$$

where S is a parameter that depends on the soil type, A_0 is the maximum effective acceleration, α is the amplification factor for each mode of vibration, R^* is the reduction factor, and I is the importance factor. The building's location was El Venado, San Pedro de la Paz, with an occupation category II (I = 1.0), seismic zone 3 (A_0 = 0.4g), and a soil type C (S = 1.05, T_0 = 0.4, T' = 0.45, n = 1.4, p = 1.6). Eq. 3-4 and 3-5 calculate factors α and R^*, respectively

$$\alpha = \frac{1 + 4.5(T_n/T_0)^p}{1 + (T_n/T_0)^3} \qquad \text{Eq. 3-4}$$

$$R^* = 1 + \frac{NR_0}{4T_0R_0 + N} \qquad \text{Eq. 3-5}$$

where T_n is the period of vibration of the mode n and T_0, p are parameters that depend on the soil type, and N is the number of stories in the building. Fig. 3.3 shows the design spectrum obtained with these equations.

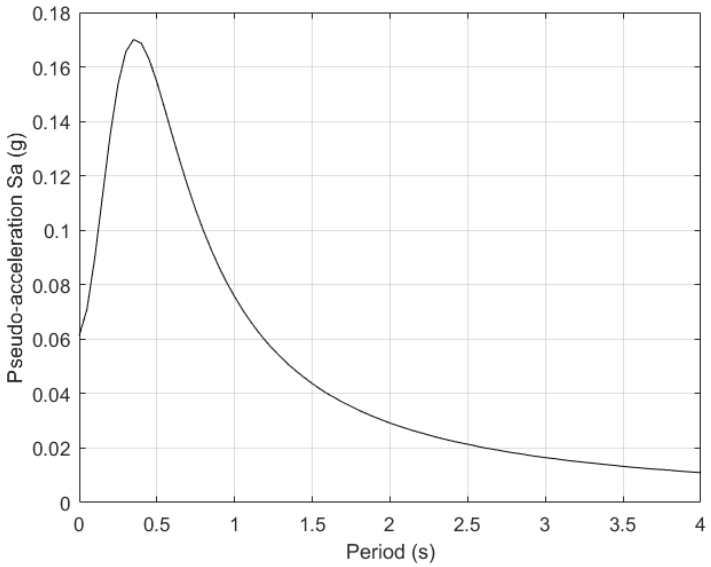

Fig. 3.3. NCh433+DS61 design spectrum.

Periods in each principal direction of analysis were T_x = 0.784 s and T_y = 1.233 s, which were obtained directly from the model. The DS60 requires the following elastic displacement spectrum S_{de} for the design of RC slender walls

$$S_{de}(T_n) = \frac{T_n}{4\pi^2}\ \alpha\ A_0\ C_d^* \qquad \text{Eq. 3-6}$$

where S_{de} is the elastic displacement spectrum in cm, A_0 is in cm/s^2 units, and C_d^* is soil-type dependant and takes the following values for a soil-type C

$$C_d = \begin{cases} 1.0 & \text{for } T_n \le 0.65\ s \\ 0.57T_n + 0.63 & \text{for } 0.65\ s \le T_n \le 2.02\ s \\ 0.055T_n^2 - 0.63T_n + 2.83 & \text{for } 2.02\ s \le T_n \le 5.00\ s \end{cases} \qquad \text{Eq. 3-7}$$

NCh433 (INN, 2012) defines the minimum and maximum base shear calculated as follows

$$Q_{mín} = \frac{I\ S\ A_0\ P}{6g}, \qquad Q_{máx} = I\ C_{máx}\ P \qquad \text{Eq. 3-8, 3-9}$$

where P is the seismic building weight over the basal level, and $C_{máx} = 0.35\ S\ A_0\ /g$ for a reinforced concrete shear wall building (R = 7). When the base shear does not lay between these two values, the obtained base shear must be corrected by a factor. For the building in the study, these limit values are Q_{min} = 708 tonf and Q_{max} = 1487 tonf, and the base shear results from the model for each direction of analysis were

$$Q_x = 768\ tonf,\ \ Q_y = 484\ tonf$$

Base shear in the *y* direction was below the minimum, so seismic loads in that direction were amplified by a factor of 1.46, reaching the minimum base shear.

Finally, for the definition of the seismic loads, an accidental eccentricity of 5% was considered, adding two extra load cases for each direction regarding the symmetry of the plan view in the ETABS *Load Cases* definition as four additional loads (two in X and two in Y) setting the *Diaphragm Eccentricity* value to 0.05.

Load combinations were applied according to NCh3171 (INN, 2010), as shown in Table 3.2.

N°	Load Combination	Notes
1	1.4 DL	
2	1.2 DL + 1.6 LL	
3	0.9 DL + 1.4 SX	Three cases for SX and SY – seismic load + two extra cases considering accidental eccentricity
4	0.9 DL + 1.4 SY	
5	1.2 DL + 1.4 SX + LL	Three cases for SX and SY – seismic load + two extra cases considering accidental eccentricity
6	1.2 DL + 1.4 SY + LL	

Table 3.2. Load combinations used in the ETABS model.

3.4 Seismic response

Table 3.3 and Table 3.4 present each analysis direction's story shears and overturning moments. For simplicity, the building was divided into five height groups, each with four

stories.

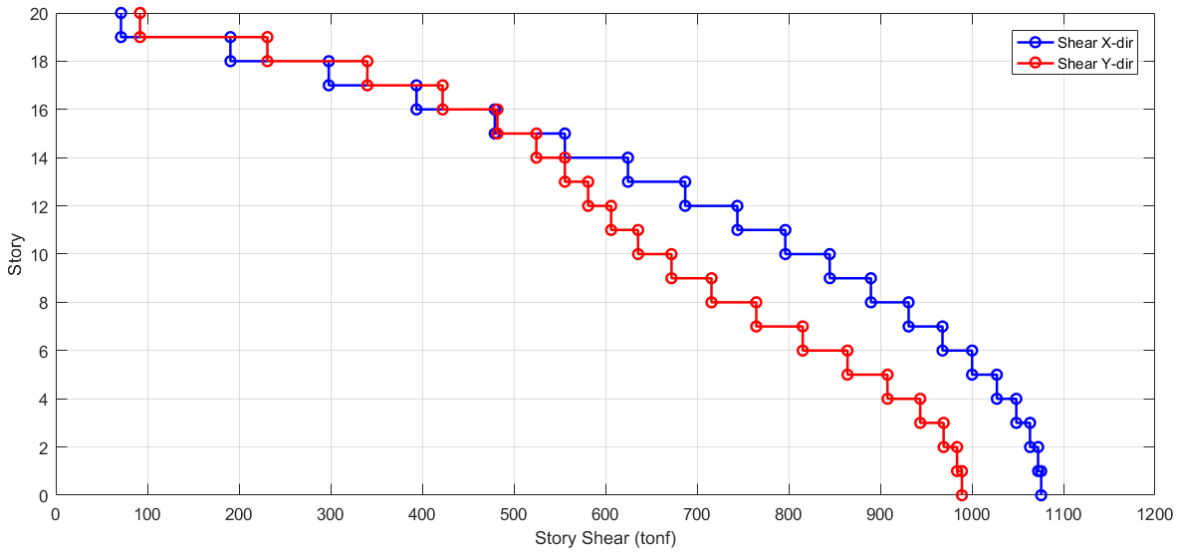

Fig. 3.4 plots the story shears.

According to NCh433, between two consecutive stories, the relative displacements at the center of mass (CM) must not exceed 0.002 times the story height, and the relative displacements at any point between these levels must not exceed 0.001 times the story height plus the relative displacement between the centers of mass of the respective stories. Table 3.5 lists the displacements for the two cases: CM displacements and for a point located in a corner. From this table, the building satisfies the NCh433 requirements.

Story	**Q_x (tonf)**	**M_y (tonf-m)**
17 – 20	394	40991
13 – 16	687	87749
9 – 12	890	137155
5 – 8	1027	188047
1 – 4	1076	239800

Table 3.3. Results for the earthquake in the X direction.

Story	**Q_y (tonf)**	**M_x (tonf-m)**
17 – 20	422	21863
13 – 16	581	47812

9 – 12	716	74260
5 – 8	908	101758
1 – 4	989	130839

Table 3.4. Results for the earthquake in the Y direction.

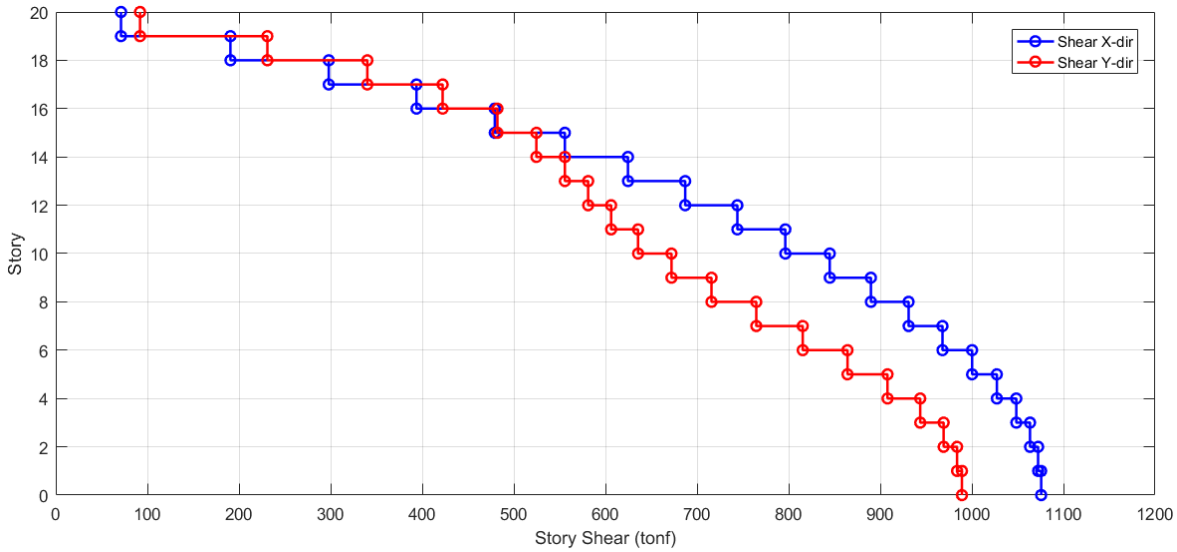

Fig. 3.4. Story shears in the X direction (blue) and Y direction (red).

Story	Max δ_{CM} = 5.2 mm				Max δ_{D1} = 2.6 mm			
	Δx_{CM} (mm)	δx_{CM} (mm)	Δy_{CM} (mm)	δy_{CM} (mm)	Δx (mm)	$\delta x - \delta x_{CM}$ (mm)	Δy (mm)	$\delta y - \delta y_{CM}$ (mm)
20	31.58	1.30	67.22	3.96	33.47	0.12	73.91	0.41
19	30.28	1.37	63.26	4.01	32.05	0.11	69.54	0.42
18	28.91	1.45	59.25	4.06	30.57	0.11	65.11	0.41
17	27.47	1.53	55.19	4.10	29.01	0.11	60.64	0.42
16	25.94	1.62	51.09	4.13	27.37	0.12	56.12	0.42
15	24.32	1.70	46.96	4.15	25.63	0.12	51.57	0.43
14	22.62	1.78	42.81	4.16	23.81	0.12	46.99	0.42
13	20.84	1.85	38.65	4.14	21.91	0.11	42.41	0.42
12	18.99	1.90	34.51	4.10	19.95	0.12	37.85	0.41
11	17.09	1.94	30.41	4.03	17.93	0.11	33.34	0.39
10	15.15	1.96	26.38	3.93	15.88	0.12	28.92	0.38
9	13.19	1.96	22.45	3.78	13.80	0.10	24.61	0.38
8	11.23	1.93	18.67	3.60	11.74	0.09	20.45	0.35
7	9.31	1.87	15.07	3.37	9.72	0.09	16.50	0.32
6	7.44	1.77	11.70	3.08	7.76	0.09	12.81	0.30
5	5.67	1.64	8.62	2.73	5.90	0.07	9.43	0.26
4	4.03	1.45	5.89	2.33	4.19	0.06	6.44	0.20
3	2.58	1.21	3.56	1.80	2.68	0.05	3.91	0.19
2	1.37	0.90	1.76	1.23	1.42	0.03	1.92	0.11
1	0.47	0.47	0.53	0.53	0.49	0.02	0.58	0.05

Table 3.5. Horizontal displacement verifications in each principal direction.

After checking the horizontal displacements in the structure, the ETABS tool *Shear Wall Design* was used to calculate the reinforcement and obtain the design forces for each wall.

3.5 Design of slender walls

DS60 (MINVU, 2011a) requires a curvature analysis to ensure ductile behavior in slender walls. Eq. 3-10 and Eq. 3-11 define the curvature demand at the wall critical section.

$$\phi_u = \frac{2\delta_u}{H_t \cdot l_w} = \frac{\varepsilon_c}{c} \leq \frac{0.008}{c} \qquad \text{Eq. 3-10}$$

$$\phi_u = \phi_e + \frac{\delta_u - \delta_e}{l_p \cdot (H_t - 0.5 l_p)} = \frac{\varepsilon_c}{c} \leq \frac{0.008}{c} \qquad \text{Eq. 3-11}$$

where H_t is the distance between the highest point of the building and the critical section, δ_u is the design displacement, c is the neutral axis depth, ϕ_e is the critical section elastic curvature, consistent with δ_e, and l_p is the plastic hinge length, which must be taken lesser or equal to $0.5l_w$. Design displacement δ_u was obtained with the displacement spectrum defined in NCh433, with the following expression

$$\delta_u = 1.3S_{de}(T_{ag}) \qquad \text{Eq. 3-12}$$

where T_{ag} is the period with the most translational mass considering the effects of reinforcing steel and concrete cracking, and can be approximated as 1.5 times the period obtained with the gross sections. The value *0.008/c* corresponds to the curvature capacity obtained with the *Section Designer* tool in SAP2000 (CSI, 2017) with the moment-curvature diagrams for the walls, considering a concrete strain of ε_c = 0.008 with vertical loads consistent with the ETABS model. Fig. 3.5 shows an example of Wall 1.

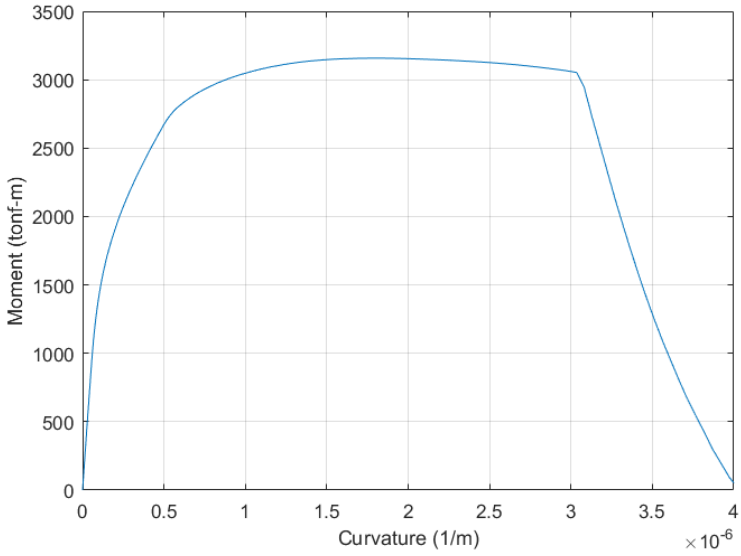

Fig. 3.5. Moment-curvature diagram for wall 1 in SAP2000.

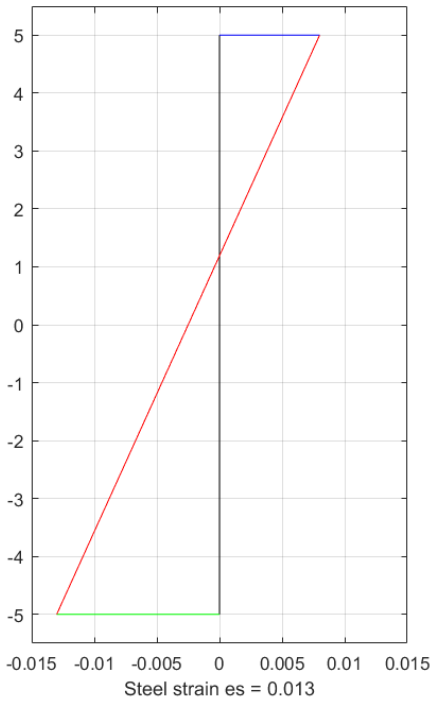

Fig. 3.6. Strain diagram for wall 1 for ε_c = 0.008.

Eq. 3-13 gives the neutral axis depth from the moment-curvature diagram in SAP2000.

$$c = \frac{\varepsilon_c}{\varepsilon_c + \varepsilon_s} \cdot l_w \qquad \text{Eq. 3-13}$$

Eq. 3-14 gives the length c_c over which confinement must be provided at wall boundaries

$$c_c = c - \frac{l_w}{600(\delta_u'/h_w')} \qquad \text{Eq. 3-14}$$

where δ_u' is the relative displacement between the highest point of the wall and the analyzed section, and h_w' is the height of the wall measured between the same two points. If this value is positive, then a special boundary element (SBE) must be used, with a specified minimum bar spacing and transverse confining reinforcement calculated with Eq. 3-15, ensuring that ε_c is between 0.003 and 0.008.

$$A_{sh} = 0.09 \frac{s\ b_c\ f_c'}{f_{yt}} \qquad \text{Eq. 3-15}$$

If c_c is negative, an ordinary boundary element (OBE) can be used, considering bar spacing specifications if the reinforcement ratio is greater than $2.8/f_y$ (MINVU, 2011a). Fig. 3.7 depicts the nomenclature used for boundary elements in T-shaped walls.

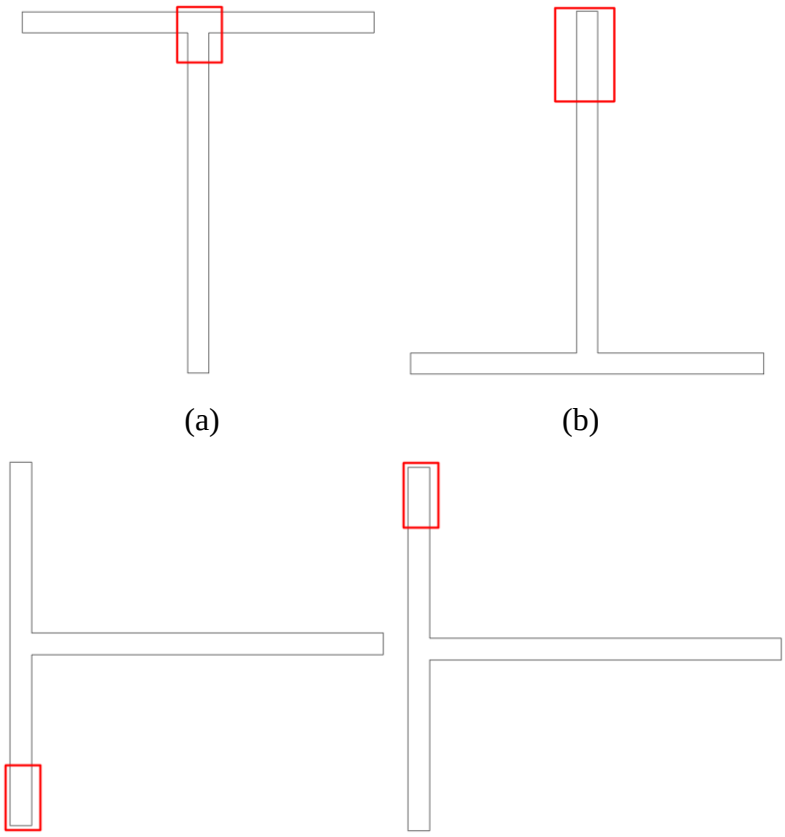

Fig. 3.7. Boundary elements in each direction for T-shaped walls: (a) 0° rotation; (b) 180° rotation; (c) 90° rotation; (d) 270° rotation.

Table 3.6 summarizes the designed reinforcement at wall boundaries. Fig. 3.8 to Fig. 3.11 present detailed drawings.

Story	**Wall 1**	**Wall 2**			**Wall 3**	**Wall 4**
		Web 0°	**Web 180°**	**Flange**		
1 – 4	12ϕ16	10ϕ16	45ϕ16	22ϕ16	14ϕ16	16ϕ16
5 – 8	10ϕ16	10ϕ16	30ϕ16	22ϕ12	12ϕ16	14ϕ16
9 – 20	10ϕ12	10ϕ12	30ϕ12	22ϕ12	12ϕ12	14ϕ12

Table 3.6. Designed reinforcement at boundary elements.

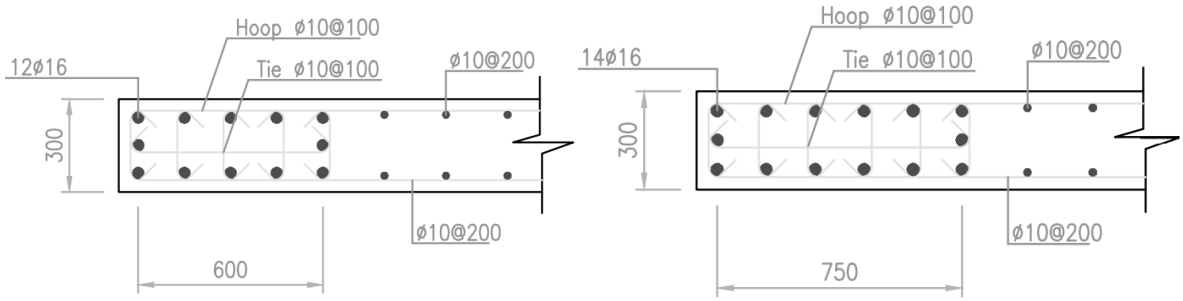

Fig. 3.8. Boundary elements for Walls 1 and 3, respectively.

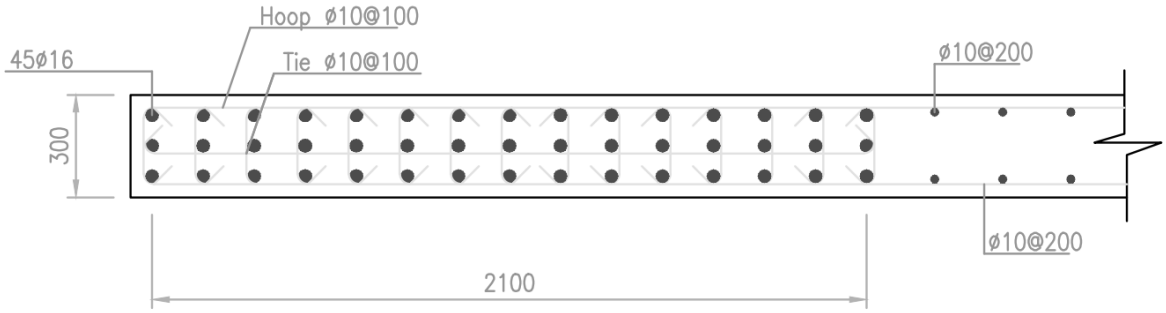

Fig. 3.9. Boundary element for Wall 2 web.

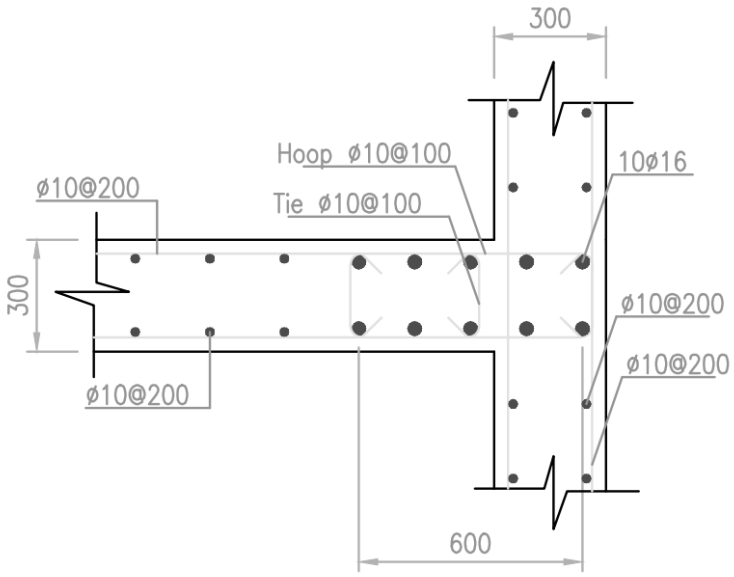

Fig. 3.10. Boundary element for Wall 2 web.

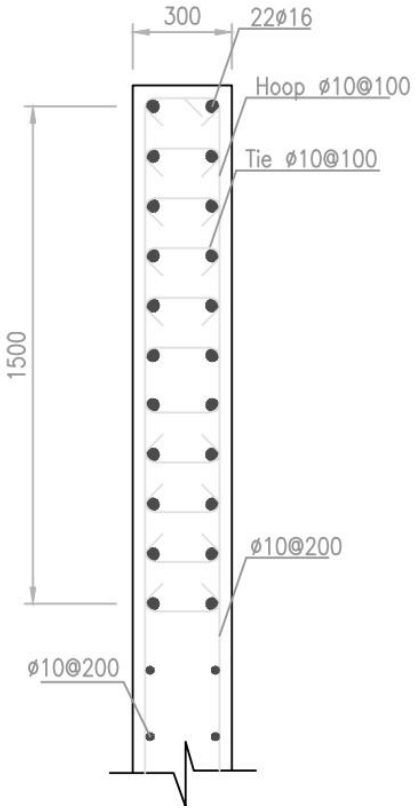

Fig. 3.11. Boundary element for Wall 2 flange.

3.6 Conclusions

NCh433+DS61 design for the studied building resulted in walls with minimum longitudinal distributed reinforcement in the web and some extra reinforcement at the boundaries, as shown in Fig. 3.8 to Fig. 3.11. The next step is verifying whether the building satisfies the ACHISINA PBEE (2017) requirements from nonlinear analyses.

CHAPTER 4 NONLINEAR MODELING OF STUDIED BUILDING

4.1 Introduction

This chapter evaluates the seismic performance of the studied building, using nonlinear analyses in the commercial software PERFORM 3D (CSI, 2016) and considering the requirements of ACHISINA (2017).

4.2 Structural modeling

Concrete constitutive curves considered three cases: confined concrete for boundary elements of each wall at the first four stories, confined concrete for boundary elements for other stories, and unconfined concrete for the remaining elements. The constitutive laws, shown in Fig. 4.1, were calculated with the Saatcioglu & Razvi (1992) proposal, as detailed in Appendix A. Then, YULRX curves were obtained for each case, following the same procedure shown in Chapter 2.

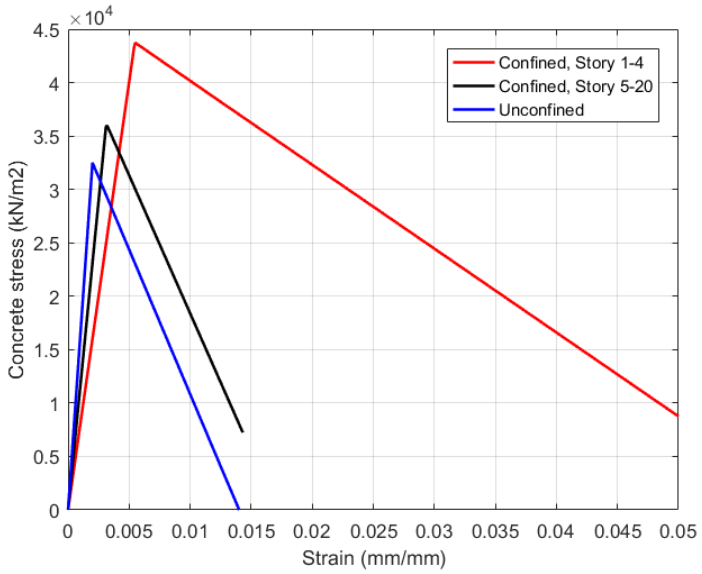

Fig. 4.1. Proposed stress-strain relationship for Wall 1 (1 kN/m^2 = 0.001 MPa).

Fig. 4.2. presents the YULRX curves for the first four stories. The proposed curves have been regularized to obtain mesh-independent results (Lowes *et al.*, 2016).

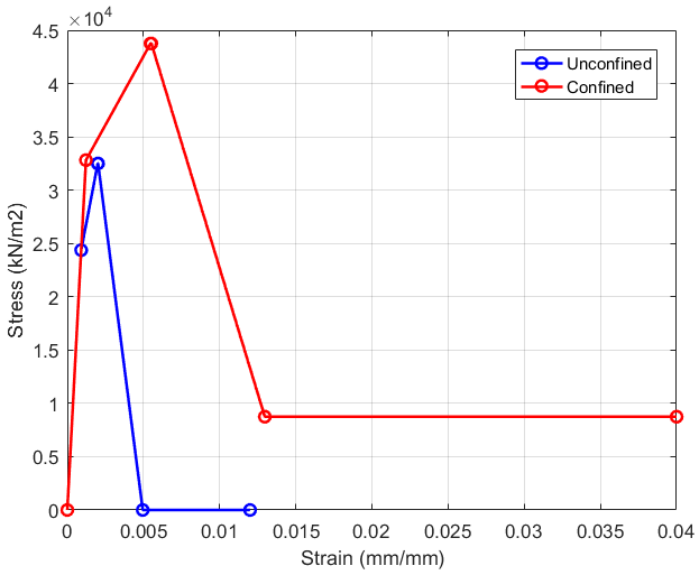

Fig. 4.2. Proposed YULRX concrete curves for the first four stories of all walls (1 kN/m^2 = 0.001 MPa).

The definition of reinforcement steel constitutive curves followed recommendations by Moehle (2003) and ACHISINA (2017) for the calculation of f_y and f_u., considering a simplified model for steel buckling, where the steel compressive capacity is lost when the concrete reaches its residual strength. Fig. 4.3 presents the steel curves.

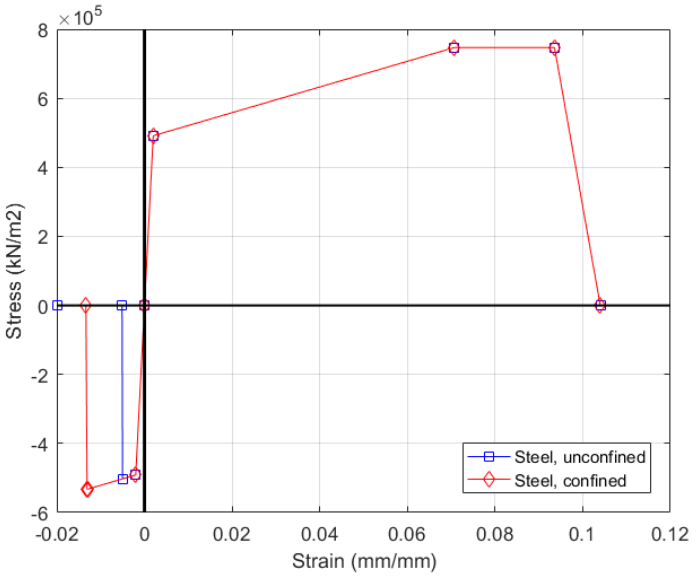

Fig. 4.3. Proposed YULRX steel curves for all walls (1 kN/m^2 = 0.001 MPa).

Shear behavior was modeled as elastic, perfectly plastic, following the same procedure as Ugalde *et al.* (2019). For the linear portion, shear stiffness was considered $0.1G_cA_{cv}$, where $G_c = 0.4E_c$ and A_{cv} is the gross wall area. For the inelastic part, Eq. 4-1 calculates the shear stress value (ACI, 2014), increasing it by 50% to represent the expected shear strength of the core walls. Fig. 4.4 shows the obtained shear stress curve.

$$\frac{V_{ult}}{A_{cv}} = 1.5\frac{V_n}{A_{cv}} = 1.5(\alpha_c\lambda\sqrt{f_c'} + \rho_t f_y) \quad \text{Eq. 4-1}$$

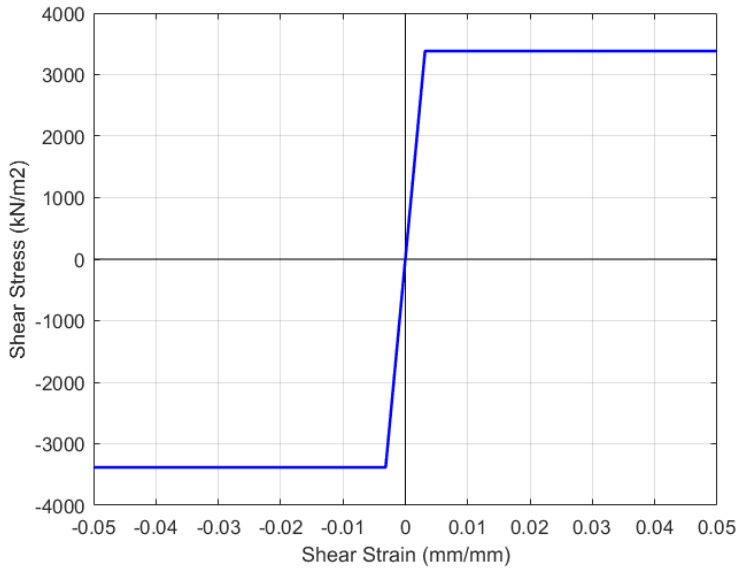

Fig. 4.4. Shear material constitutive curve for all walls (1 kN/m^2 = 0.001 MPa).

Table 2.2 indicates the cyclic degradation energy factors. The first analysis of this building did not consider slabs; instead, every story level considered rigid diaphragms and lumped masses and fixed nodes at the base. Gravity loads were added as point loads based on tributary areas.

Slender walls were meshed considering four elements in the horizontal direction (one per boundary element and two in the web) and one in the vertical direction (two for the first four stories). Only for the W2 T-shaped wall were two elements considered at the wall stem. Fig. 4.5 shows the model's respective mesh in a 3D view.

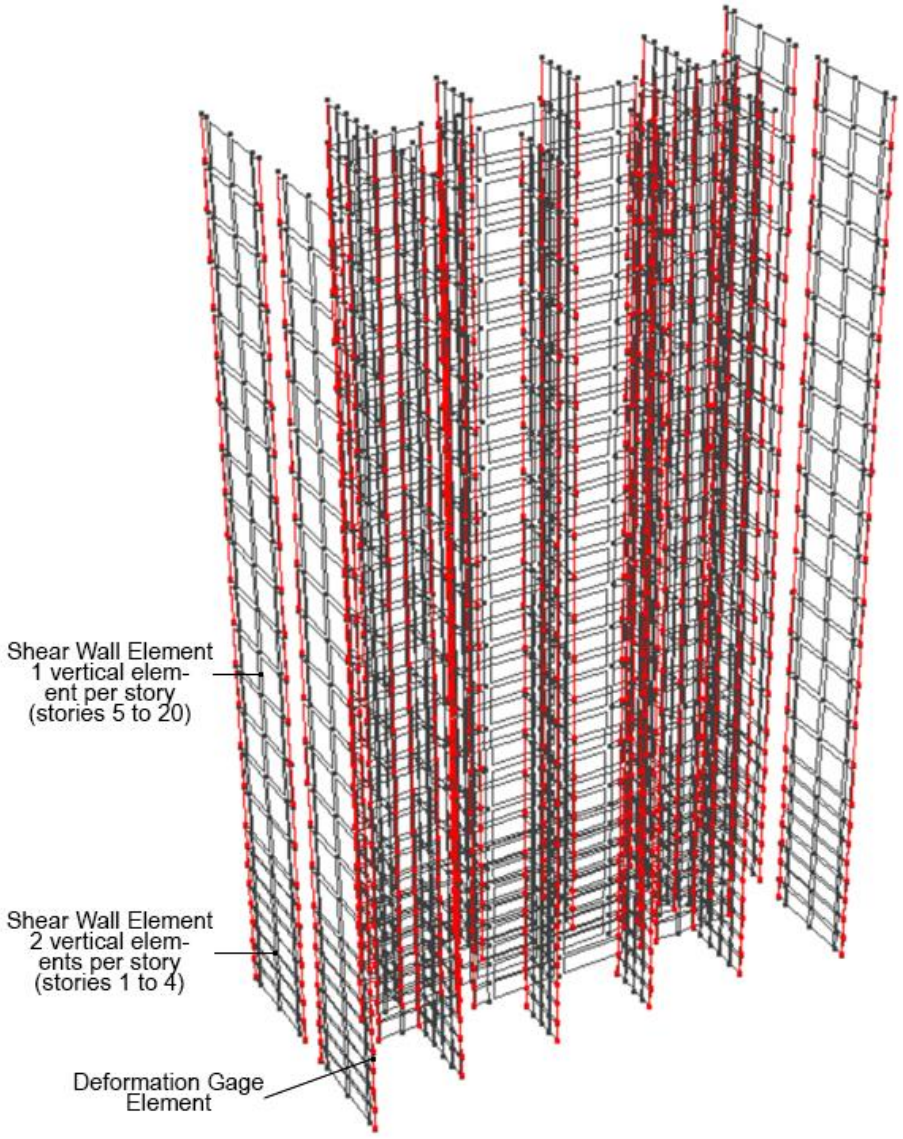

Fig. 4.5. Elements defined in the PERFORM-3D model.

Fiber models were used for each wall, manually defining the reinforcement and concrete fibers in the boundary elements and automatically defining these fibers in web elements. Out-of-plane action was assumed elastic for all structural components. In addition, two-point deformation gage elements were added at the edge of every wall at all stories to measure axial strains. Fig. 4.5 shows the location of each gage element in the model in red.

4.3 ACHISINA PBEE requirements

ACHISINA (2017) defines two seismic levels for performance-based verifications, the Design Basis Earthquake and the Maximum Considered Earthquake shortened respectively as SD and SMC for their initials in Spanish (*Sismo de Diseño* and *Sismo Máximo Considerado*). The SD can be defined with a minimum of three horizontal pairs of records, adding artificial records if there are no components of accurate records. For each ground motion, the pseudo-acceleration spectra must be made for a 5% damping ratio and combined with the Square Root of the Sum of Squares (SRSS) method. Records must be modified so that the mean of the displacement spectra of all the seismic motions combined with SRSS is not lower than 1.17 times the elastic displacement spectrum of DS61 (MINVU, 2011b) for a 5% damping ratio in a range of periods between *0.5T* and *1.25T*, where *T* is the fundamental period of the structure. Eq. 4-2 is the expression for this elastic displacement spectrum, S_d, obtained from the pseudo-acceleration spectrum (PS_a) given in NCh433 for reinforced concrete buildings based on the properties listed in the previously mentioned provisions.

$$S_d = \frac{T_n^2}{4\pi^2} PS_a \qquad \text{Eq. 4-2}$$

Alternatively, the document states that the SD can be obtained through a site-specific seismic hazard analysis considering a return period of T_r = 475 years, equivalent to a probability of exceedance of 10% in 50 years. The SD limit state verification requires a nonlinear response-history analysis and must meet an Immediate Occupancy performance level, where the building essentially maintains its pre-earthquake properties and is safe to occupy. The used load combination for the structure is $1.0\ D + L_{exp} + 1.0\ SD$, where *D* is the permanent dead load, and L_{exp} is the expected live load, taken as 25% of the live load. If there are at least seven pairs of records, the parameter of interest can be taken as the mean value of the results. If there are six or fewer ground motions, the maximum value of the parameter of interest is used.

The SD records can be amplified by 30% for the SMC. Alternatively, the SMC can be obtained through a site-specific seismic hazard analysis considering a return period of T_r = 950 years, equivalent to a probability of exceedance of 10% in 100 years. Additionally, a

pushover analysis that leads the structure to a roof displacement 40% greater than the roof displacement obtained in the SD can apply as the SMC. The limit state for the SMC gives the structure an additional deformation capacity for earthquakes that exceed the SD. Table 4.1 summarizes the acceptance criteria for each limit state.

Element/Criteria	**SD limit**	**SMC limit**
1. Local acceptance criteria		
Force-controlled elements must meet	$\lambda F_u \leq \phi F_n$	$F_u \leq \phi F_n$
Deformation-controlled elements must meet the following:		
Compression strain in confined concrete	0.008	0.015
Compression strain in unconfined concrete	0.003	0.003
Tension strain in reinforcement steel	0.030	0.050
2. Global acceptance criteria		
Story drift for buildings with fragile non-structural elements	0.005	n.a.
Story drift for buildings with ductile non-structural elements	0.007	n.a.

Table 4.1. Values for each limit state in reinforced concrete walls (ACHISINA, 2017).

For force-controlled elements, F_u and F_n are the demand and nominal strength of the material according to the design code, respectively, considering λ = 1.5 and ϕ = 1.0 for all force-controlled elements. Unlike the SD, the SMC does not require a story drift check; the global acceptance is considered implicitly in the local criteria.

Pairs of records were selected from the SIBER-RISK Strong Motion Database (Castro *et al.*, 2020), considering only subduction records with a magnitude M_w larger than 6.5 and using the GMRotD50 (Boore *et al.*, 2006) combination of the two horizontal components to match the target spectrum (NCh433+DS61).

Fig. 4.6 presents the flowchart for the selection of records for analysis. Amplifying factors greater than ten were discarded, as they may differ significantly from the actual earthquake motion. The ACHISINA document establishes a minimum of three pairs of records, and these records must satisfy that the mean of their SRSS-combined spectra is greater than 1.17 times

the target spectrum. Fig. 4.7 shows this verification considering five seismic records. Table 4.2 lists the selected earthquakes and corresponding amplification factors.

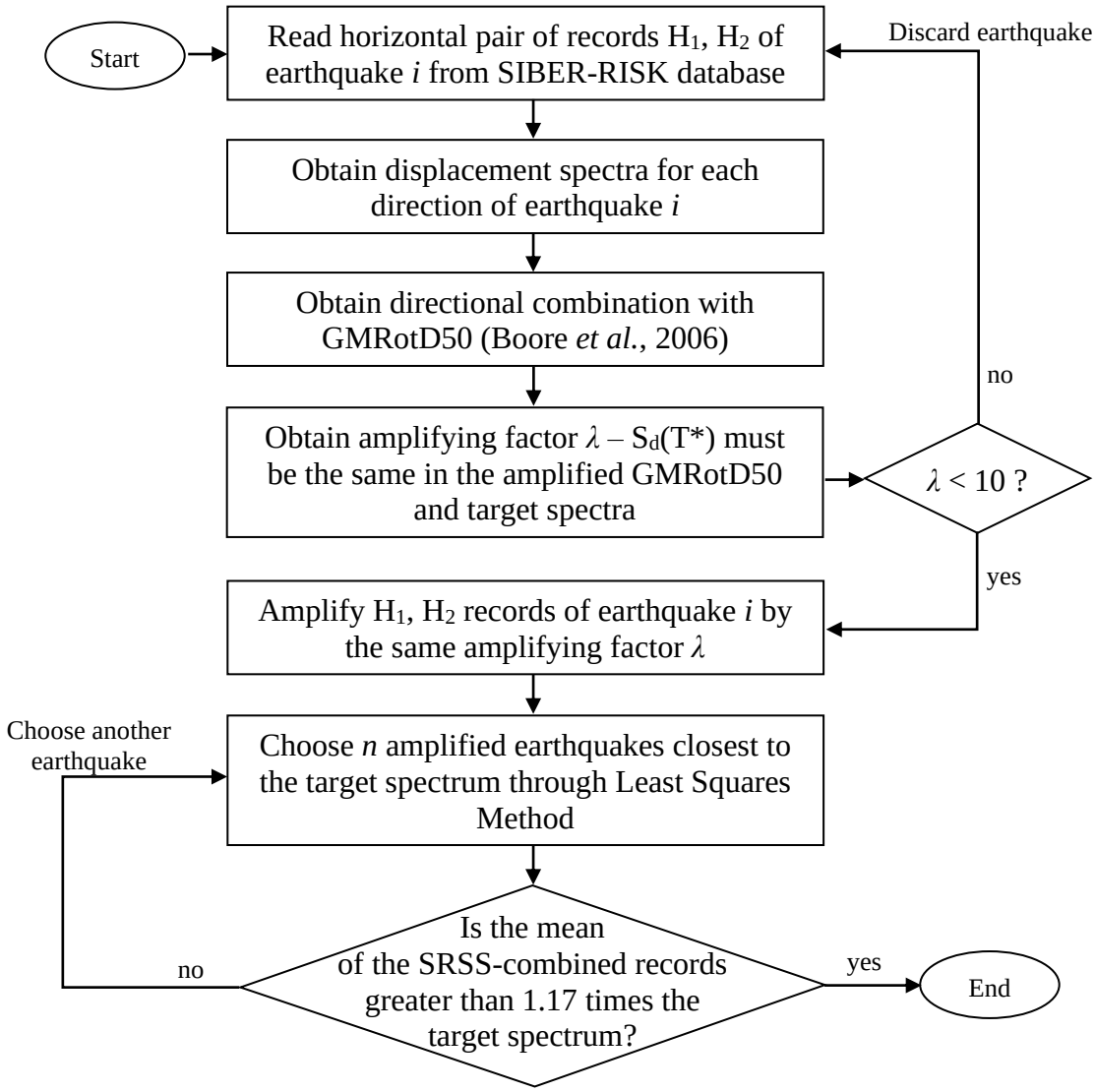

Fig. 4.6. Earthquake record selection flowchart.

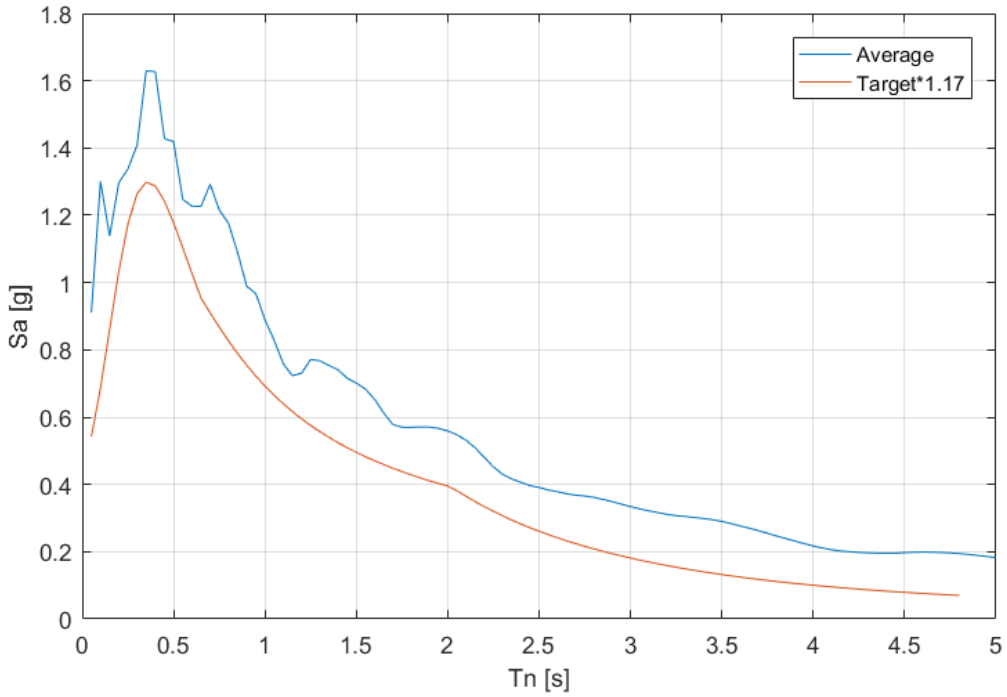

Fig. 4.7. SRSS-combined mean of the displacement spectra for the chosen earthquakes.

Record	M_w	Location	Year	Amplification factor λ
1	7.9	33.95 S, 71.71 W	1985	7.74
2	7.2	17.53 S, 72.07 W	2001	5.97
3	6.7	22.33 S, 70.06 W	2007	5.23
4	6.8	23.04 S, 70.18 W	2007	6.31
5	6.7	22.33 S, 70.06 W	2007	3.48

Table 4.2. Selected records from the SIBER-RISK (2020) database.

4.4 Conclusion

The chapter introduced the approach followed for nonlinear building modeling. Seismic records were selected from an extensive database of Chilean subduction earthquakes database, all of them suited for nonlinear analysis. ACHISINA requirements for performance-based verification were introduced. The next chapter presents the results of nonlinear analysis and performance verifications.

CHAPTER 5 EVALUATION OF ACHISINA PBEE REQUIREMENTS

5.1 Introduction

This chapter presents the results from the nonlinear analyses and the evaluation of the studied building according to the ACHISINA PBEE methodology. If the code-based designed building satisfies the performance-based criteria, some design changes will be proposed based on the ACHISINA guidelines to reduce the project costs.

5.2 Modal pushover analysis results

Table 5.1 compares the fundamental periods in each analysis direction obtained from three different models: i) ETABS linear-elastic model (including slabs modeling), considered for the building design, ii) ETABS linear-elastic model (excluding explicit modeling of slabs) and iii) PERFORM 3D nonlinear model (excluding explicit modeling of slabs). Models that do not include slabs show similar periods, while the linear model that considers slabs used for the building design exhibits a higher stiffness.

Linear model with slabs		**Linear model w/o slabs**		**Nonlinear model w/o slabs**	
T_x (s)	0.784	**T_x (s)**	1.603	**T_x (s)**	1.704
T_y (s)	1.233	**T_y (s)**	1.781	**T_y (s)**	1.774

Table 5.1. Fundamental periods for different models.

Fig. 5.1 presents the results from modal pushover analyses conducted on the two main building directions, using the fundamental mode for each case. The red-dotted line corresponds to the design base (V_d), obtained with the reduced spectrum from NCh433+DS61. Eq. 5-1 defines the overstrength (Ω) and is approximately 1.20 for both analyses, where V_{max} is the maximum lateral force in each case.

$$\Omega = \frac{V_{max}}{V_d} \qquad \text{Eq. 5-1}$$

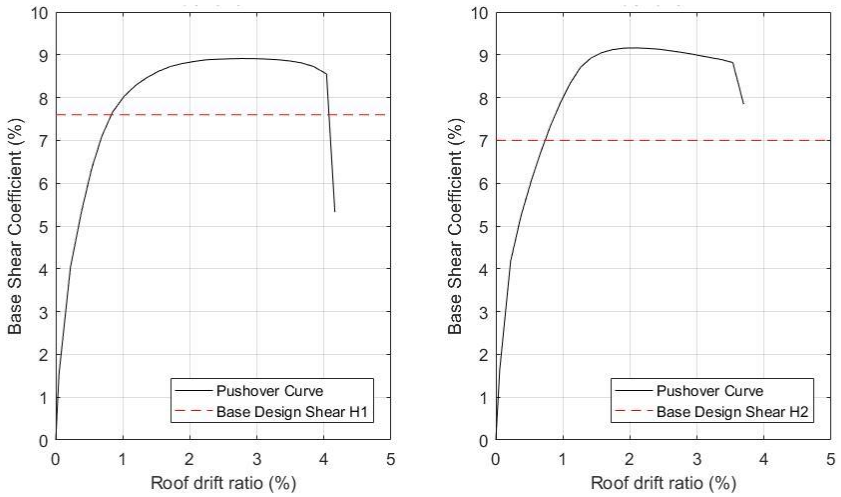

Fig. 5.1. Pushover curves in the study building's longitudinal direction (H_1) and the transverse direction (H_2).

Cando *et al.* (2020) obtained an overstrength of 2.6 for a similar building. However, their nonlinear model explicitly included a portion of the slab, modeled as a linear elastic frame element with reduced stiffness to consider cracking. Ugalde *et al.* (2019) studied the effects of slab modeling in the nonlinear response of shear wall buildings, showing that modeling without slabs and only considering rigid diaphragms at each story level reduces the peak of the pushover curve. Modeling with slabs gives peak pushover values 1.6 to 2.5 times the obtained without slabs, even with reduced stiffness (Ugalde *et al.*, 2020).

5.3 Dynamic analysis results

The compressive and tensile strains at wall edges and the maximum story drift ratio were obtained for each seismic record to compare them with the ACHISINA limits established in the previous chapter. Fig. 5.2 presents the corresponding flowchart.

Fig. 5.3 compares the envelope of maximum compressive and tensile strains at wall edges versus the maximum values to meet the performance objectives established by ACHISINA. Wall 1, 2, and 3 satisfy the strain limits for the SD state (Table 4.1); however, Wall 4 does not fulfill the requirement, reaching a tensile strain of approximately 0.04 at the base level.

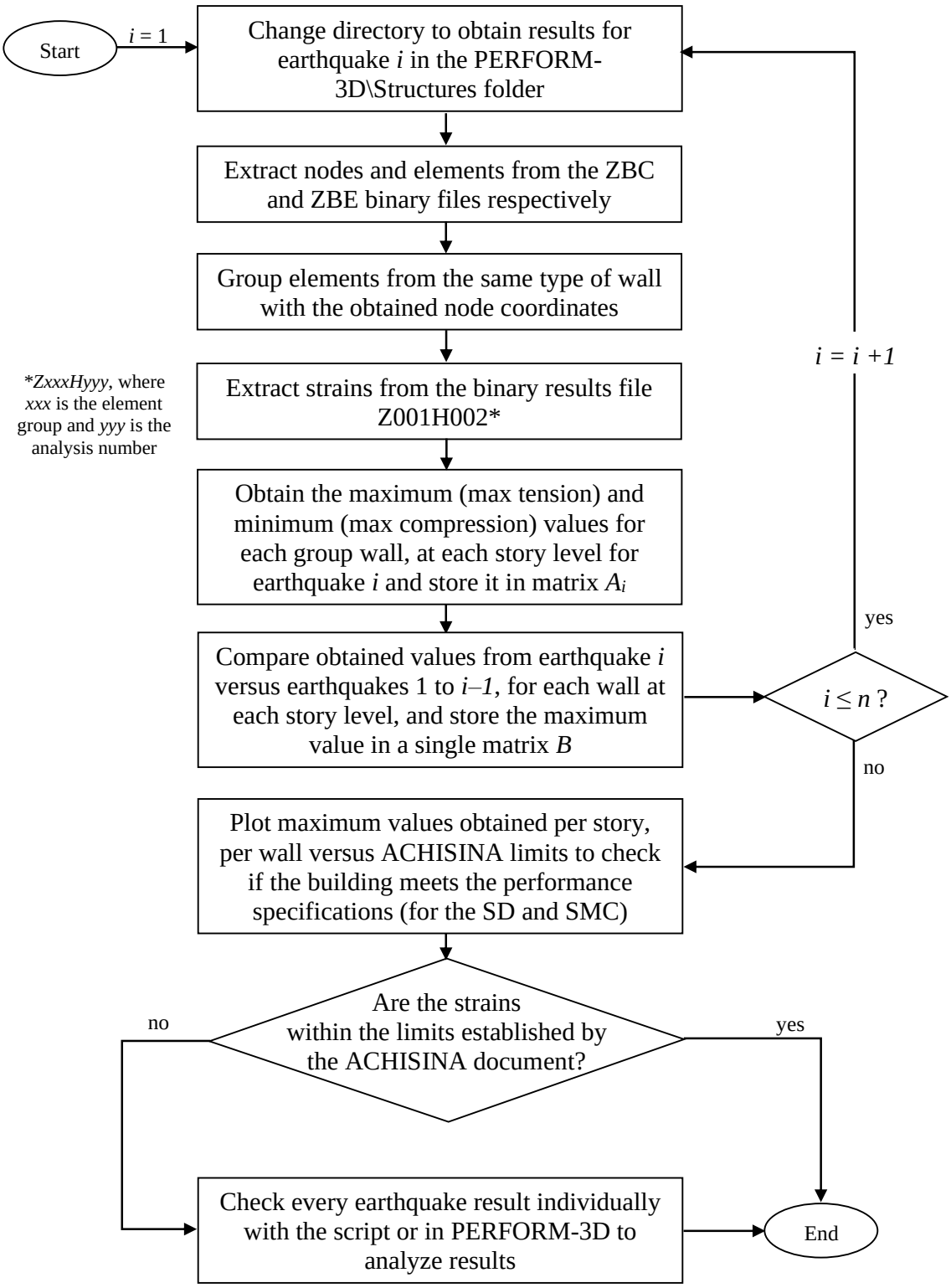

Fig. 5.2. Flowchart for Deformation Gage element results through PERFORM-3D binary files.

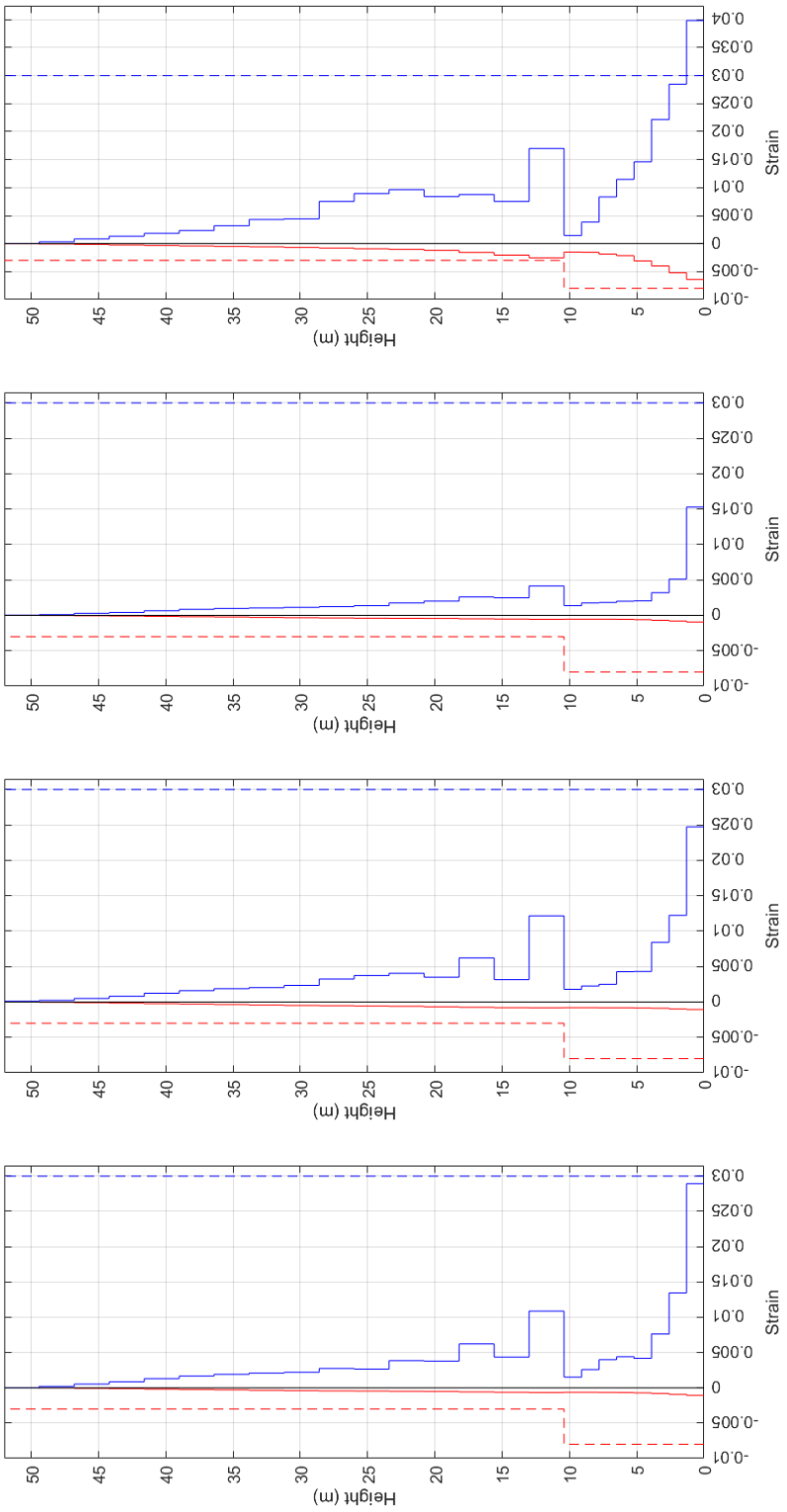

Fig. 5.3. Strain profiles for Walls 1, 2, 3, and 4 for the SD group versus ACHISINA limits, respectively.

For every wall group, there is an increase in the strains between stories 4 and 5, where the detailing at the wall edges changes from special to ordinary boundary elements, resulting in a sudden change of stiffness and a stress concentration at that level.

All walls satisfy the shear requirements at the SD level, considering them as force-controlled elements for this case, as shown in Table 5.2.

SD (λ = 1.5)	**Wall 1**	**Wall 2 (H_1)**	**Wall 2 (H_2)**	**Wall 3**	**Wall 4**
Max λ V_u (ton)	425	584	549	212	1279
ϕ V_n (ton)	880	678	678	473	1490
λ V_u / ϕ V_n	0.48	0.86	0.81	0.45	0.86

Table 5.2. Maximum shear values obtained for all SD earthquakes per wall group.

For the global acceptance criteria for the SD, story drifts were obtained at the center of mass at each story level for each earthquake and plotted as an envelope considering the maximum values versus the limits established by ACHISINA. Fig. 5.4 shows these results, showing that the building does not satisfy these requirements in both directions.

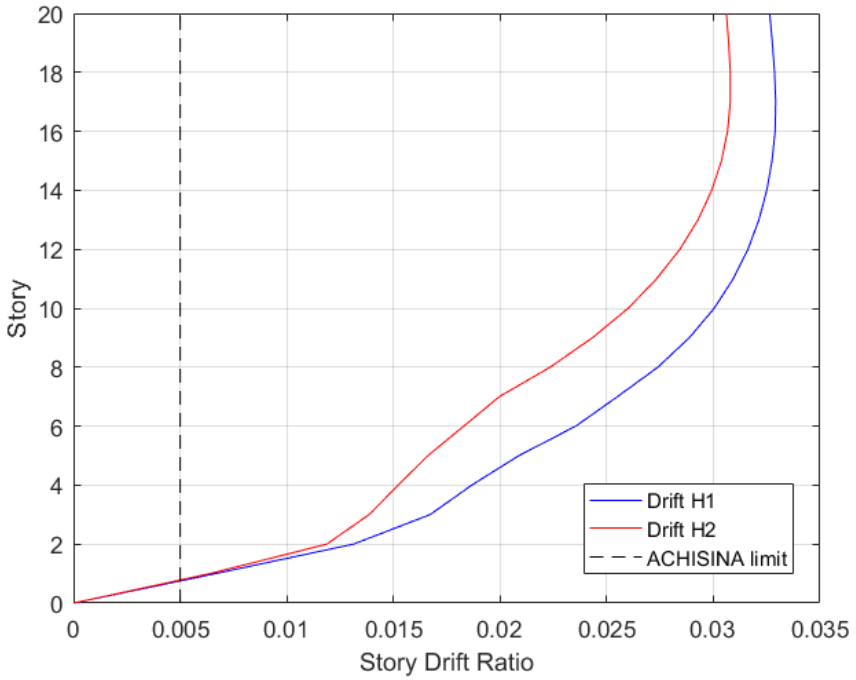

Fig. 5.4. Maximum story drifts at each story level versus ACHISINA limits.

The SMC records considered for analysis were the SD records amplified by 1.3 to check if the building satisfies the performance limits established for that ground motion.

After running these analyses, two different walls presented compressive failures for two records: Wall group 1, at the fifth story level for SMC record 2, and Wall group 4, at the base for SMC record 5. Failure for the first case may occur due to the change in stiffness between stories 4 and 5, and for the second case, due to high compressive and lateral forces, considering that this same wall did not satisfy the strain limits for the SD earthquake.

Finally, as these records did not satisfy the performance objectives, alternative modeling approaches were considered to check if the building met the ACHISINA PBEE requirements without changing the code-based design.

5.4 Evaluation of alternative modeling approaches

The first alternative approach is applying spectral matching to the seismic records (Seismosoft, 2022) to match the target spectrum better.

Fig. 5.5 shows the response spectra of original records used in nonlinear analysis, while Fig. 5.6 presents the response spectra of the matched records.

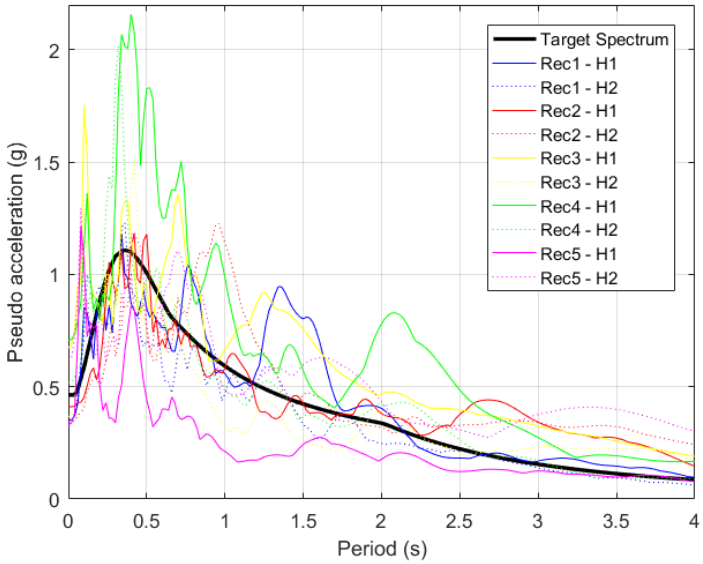

Fig. 5.5. Response spectra for the original earthquakes in each direction.

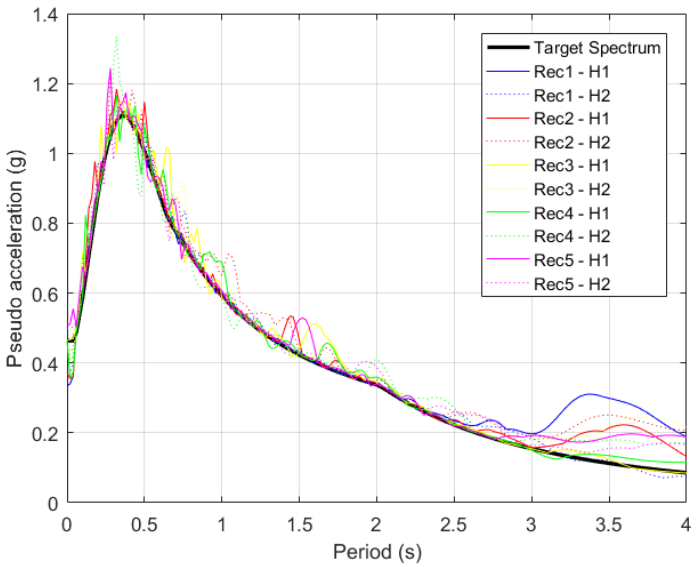

Fig. 5.6. Response spectra for the matched earthquakes in each direction.

An advantage of the spectrally matched records is the decreased seismic demand for lower periods, however, the record-to-record variability is reduced. Fig. 5.7 illustrates the ACHISINA requirement of the mean of the SRSS-combined directional spectra for these newly matched records.

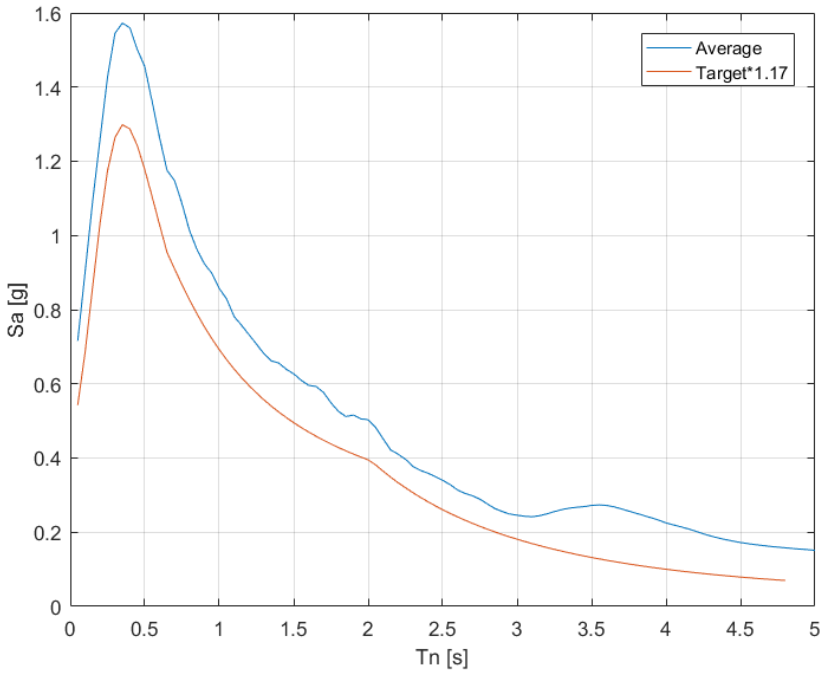

Fig. 5.7. SRSS-combined mean of the spectra for the matched earthquakes.

Results for these new records follow the same format as the previous subchapter. Fig. 5.8 and Fig. 5.9 present the maximum compressive and tensile strains at the wall edges for the SD and SMC levels. These matched records satisfy the criteria for deformation-controlled elements (Table 4.1).

For the SD, the tension strains at each wall with the matched records are lower than with the original motions, and the compressive strains increase slightly, as clearly shown on walls 2 and 4 in the fifth story. Furthermore, this sudden strain increase between stories 4 and 5 for these groups of earthquakes also occurs with these records, further indicating that this phenomenon comes from the sudden steel detailing change between confined and unconfined concrete elements generating a “rigid base” effect.

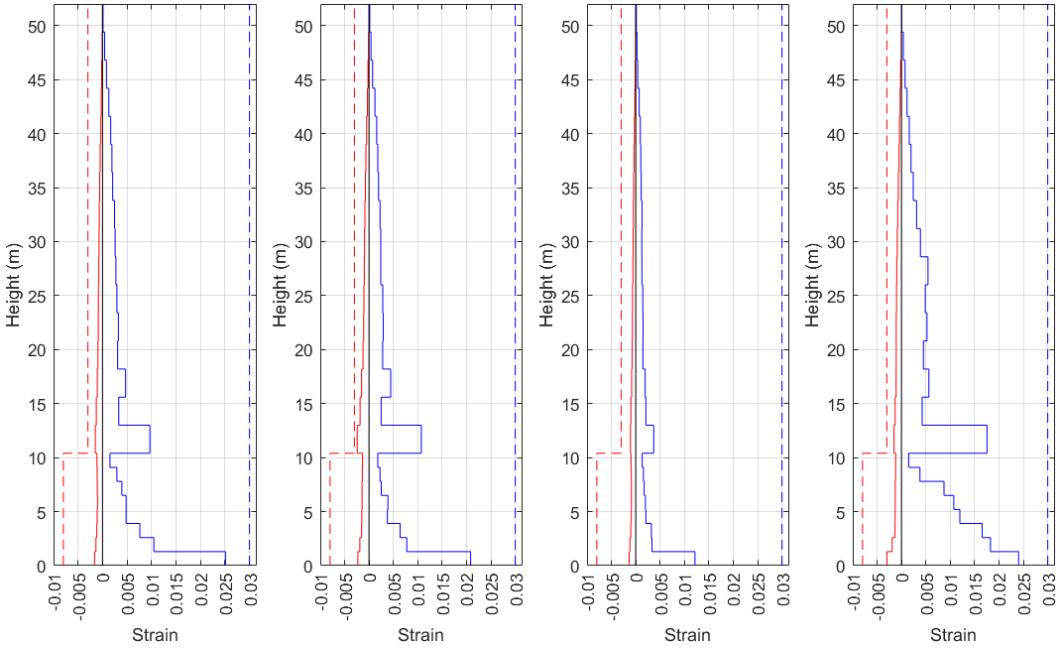

Fig. 5.8. Strain profiles for Walls 1, 2, 3, and 4 for the SD-matched records.

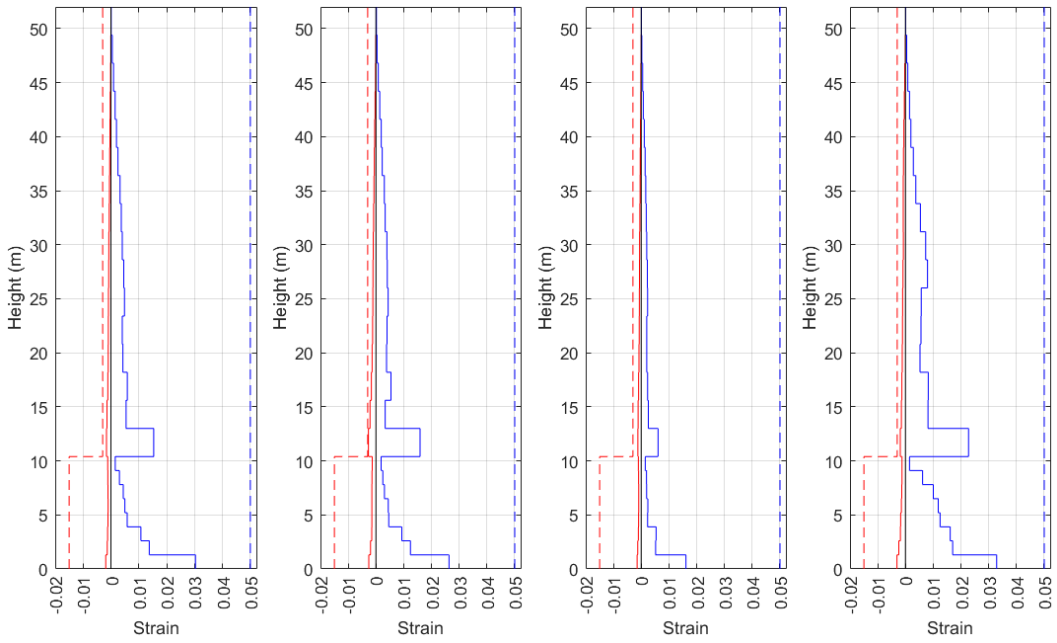

Fig. 5.9. Strain profiles for Walls 1, 2, 3, and 4 for the amplified matched records (SMC).

Table 5.3 and Table 5.4 summarize the shear results for the matched SD and the amplified SMC records with overall successful performance. Wall 2 presents the highest demand over capacity ratio values in both directions for both groups of earthquakes.

SD (λ = 1.5)	**Wall 1**	**Wall 2 (H_1)**	**Wall 2 (H_2)**	**Wall 3**	**Wall 4**
Max λV_u (ton)	512	518	592	240	1116
ϕV_n (ton)	880	678	678	473	1490
$\lambda V_u / \phi V_n$	0.58	0.76	0.87	0.51	0.75

Table 5.3. Maximum shear values obtained for all matched SD earthquakes per wall group.

SMC (λ = 1.0)	**Wall 1**	**Wall 2 (H_1)**	**Wall 2 (H_2)**	**Wall 3**	**Wall 4**
Max λV_u (ton)	389	360	471	193	855
ϕV_n (ton)	880	678	678	473	1490
$\lambda V_u / \phi V_n$	0.44	0.53	0.69	0.41	0.57

Table 5.4. Maximum shear values obtained for all SMC earthquakes per wall group.

Finally, for the global acceptance criteria for the SD, Fig. 5.10 presents the maximum story drifts. These drifts are lower than the ones obtained for the original records but exceed the ACHISINA limit of 0.005 by a large margin, increasing from 0.008 in the first story to approximately 0.025 in the last four stories in both directions.

To summarize, the SD records with spectral matching (matched records) and the respective amplified SMC records (1.3 times the SD records) have a better local response than the original records, satisfying almost all of the criteria specified by the ACHISINA document. However, the building does not meet the global acceptance criterion for the SD; thus, the response is unacceptable for this earthquake.

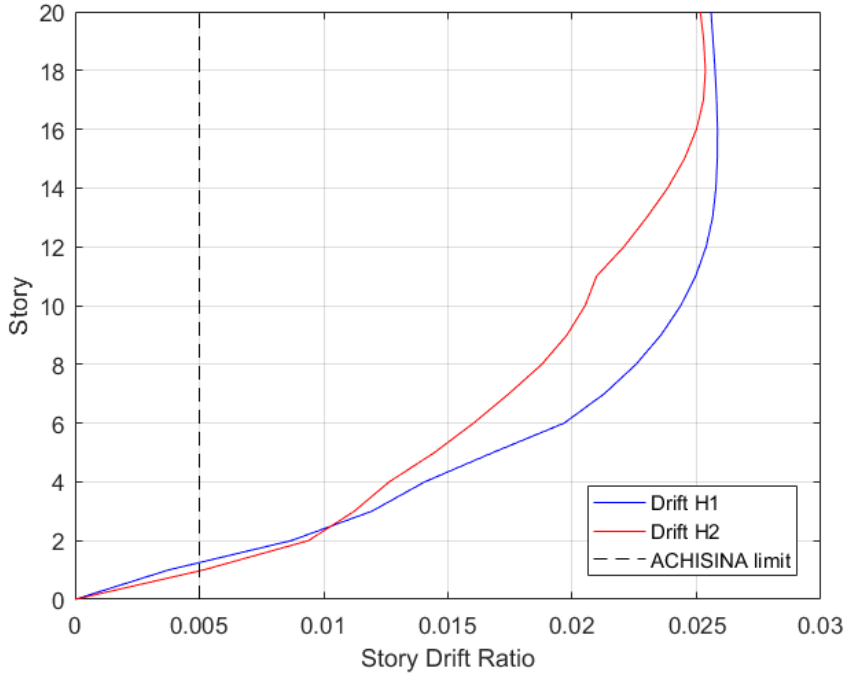

Fig. 5.10. Maximum story drifts at each story level for the matched SD records.

The second alternative approach considers the model with slabs at each story level, based on the results from subchapter 5.2 and Ugalde *et al.* (2019), applying the same matched records, which increases the lateral structure stiffness and adds a wall coupling effect. These slabs are modeled with an elastic material, considering 25% of the gross inertia following ACHISINA (2017) recommendations and Ugalde *et al.* (2020) results. Fig. 5.11 illustrates the finite element mesh for the slab elements.

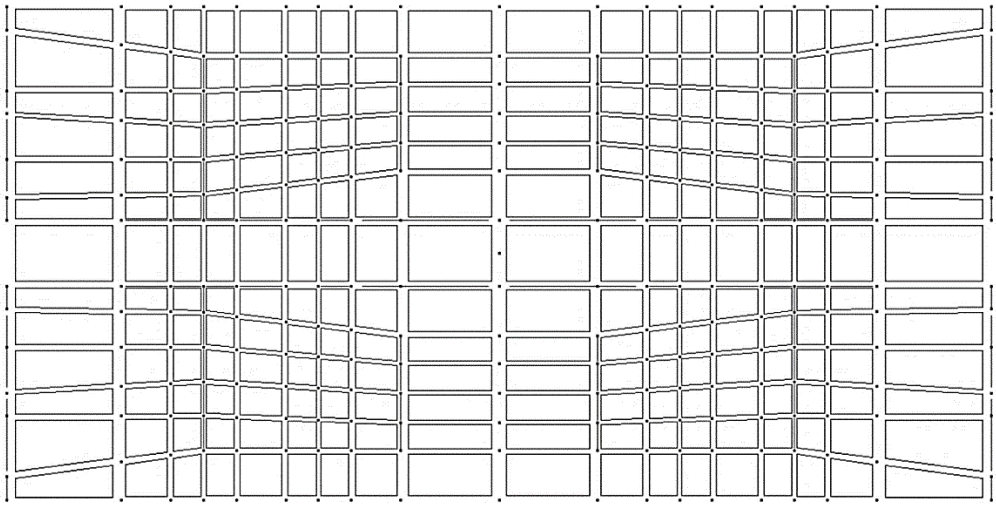

Fig. 5.11. Finite element for the slab elements for the second iteration of the model.

Fig. 5.12 and Fig. 5.13 present the strain gage results for the SD and the SMC, respectively. Walls 1, 2, and 3 meet the ACHISINA strain requirements for both groups of earthquakes, but for Wall 4, tensile strains exceed the limit value for the SD, and compression strains exceed the limit value for the SMC.

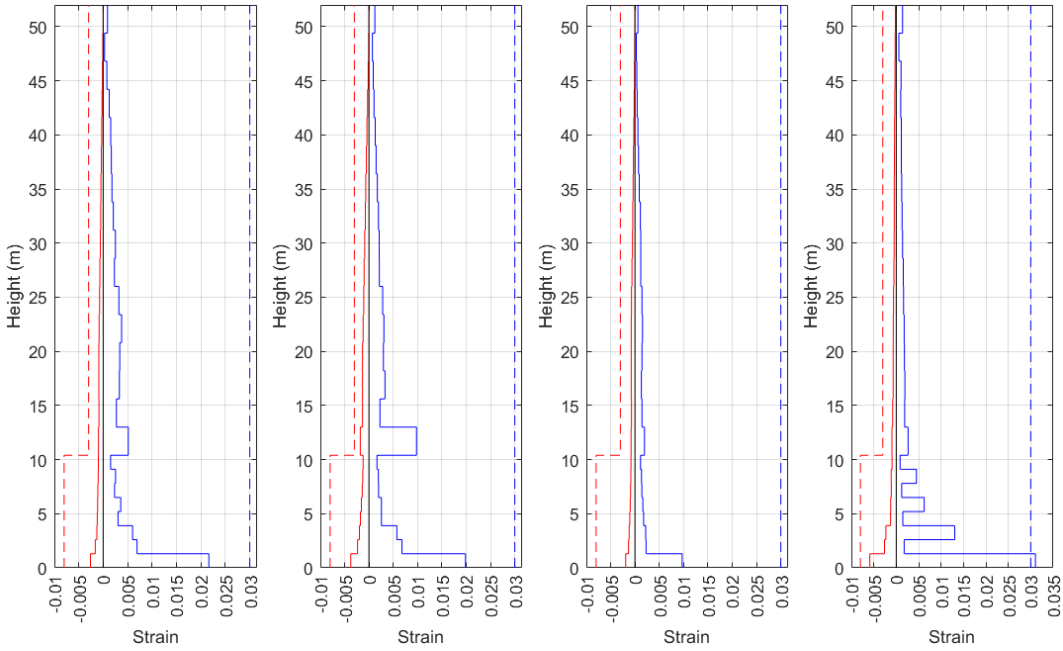

Fig. 5.12. SD strain profiles for Walls 1, 2, 3, and 4 for the model with elastic slabs.

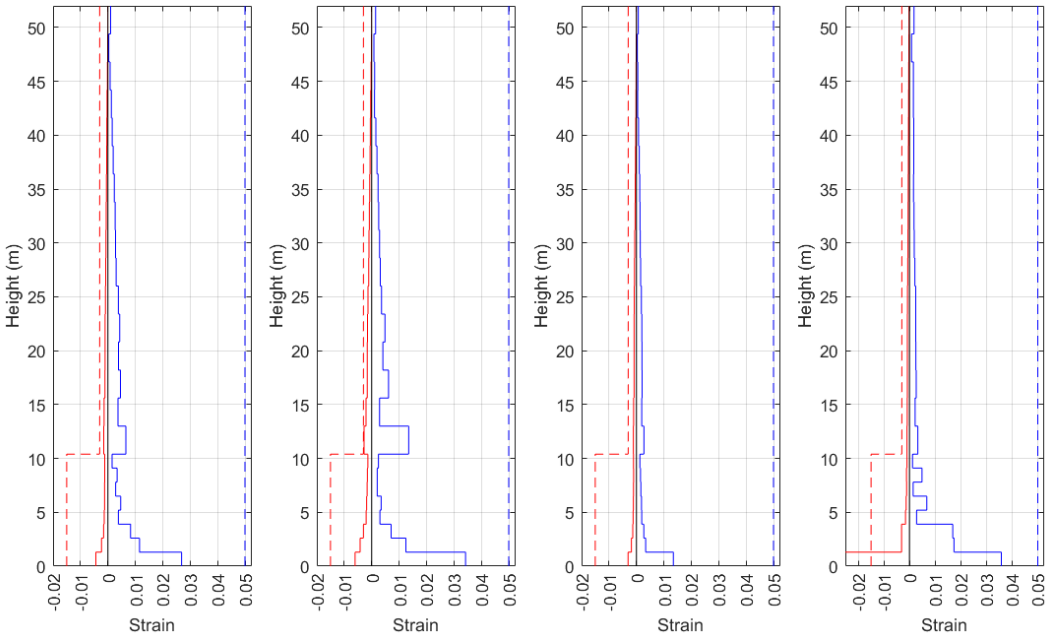

Fig. 5.13. SMC strain profiles for Walls 1, 2, 3, and 4 for the model with elastic slabs.

Strains for walls 1, 2, and 3 are similar to the ones obtained without modeling the slabs for both groups of records. However, for records 2, 3, 4, and 5, gages at the base of Wall 4 (gages 625 and 649) end with a residual compression strain, as shown in Fig. 5.14, which shows gage strains for SMC records 1-4 to compare. This could happen because of the wall length, its finite element mesh, and the re-distribution of internal stresses due to the slab coupling effect.

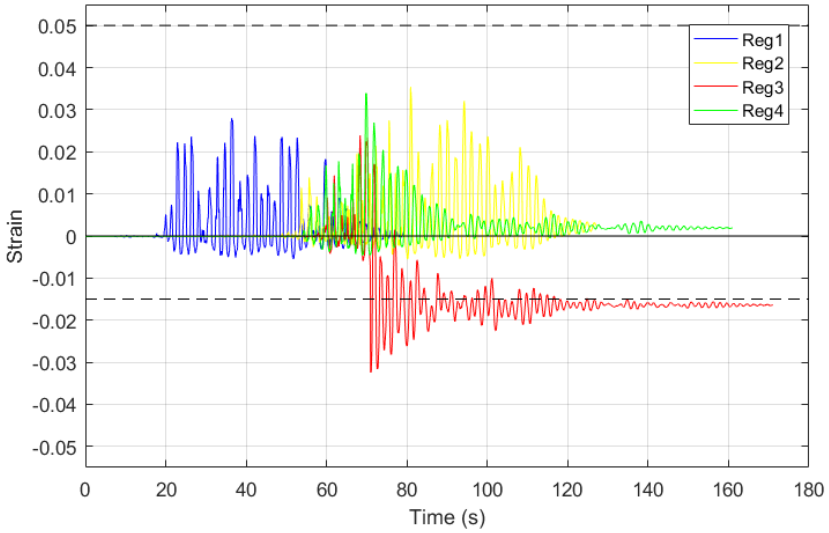

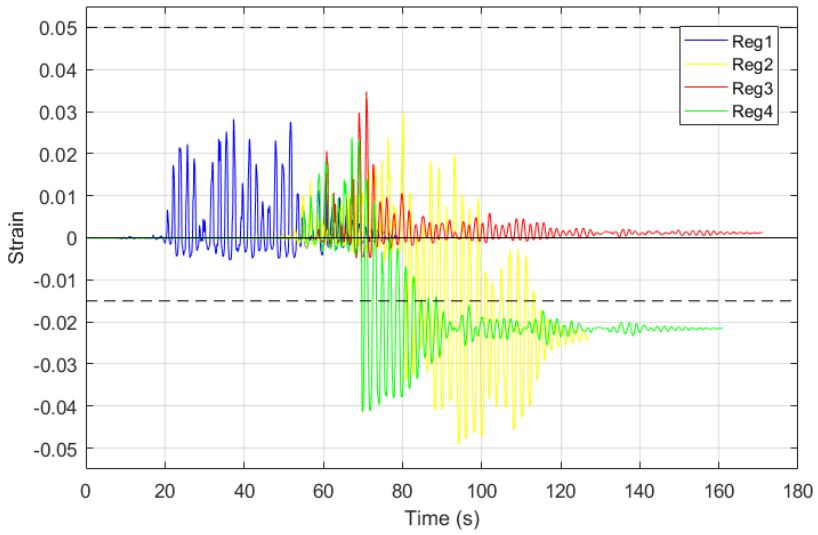

Fig. 5.14. Strains over time for records 1 to 4 in (a) gage element 625, and (b) gage element 649 (both at the base of wall 4).

Table 5.5 and Table 5.6 present the shear results for this modeling approach. Maximum shear forces present an overall increase compared to the model without slabs because of their coupling effect, exceeding the limit established for ACHISINA for the SD in wall 4. Fig. 5.15 shows the story drift results for the SD, obtaining lesser values than the model without slabs, although it still exceeds the ACHISINA limit.

SD (λ = 1.5)	**Wall 1**	**Wall 2 (H_1)**	**Wall 2 (H_2)**	**Wall 3**	**Wall 4**
Max λV_u (ton)	597	643	677	256	1748
ϕV_n (ton)	880	678	678	473	1490
$\lambda V_u / \phi V_n$	0.68	0.95	1.00	0.54	1.17

Table 5.5. Maximum shear values obtained for all SD earthquakes per wall group.

SMC (λ = 1.0)	**Wall 1**	**Wall 2 (H_1)**	**Wall 2 (H_2)**	**Wall 3**	**Wall 4**
Max λV_u (ton)	446	502	591	177	1251
ϕV_n (ton)	880	678	678	473	1490
$\lambda V_u / \phi V_n$	0.51	0.74	0.87	0.37	0.84

Table 5.6. Maximum shear values obtained for all SMC earthquakes per wall group.

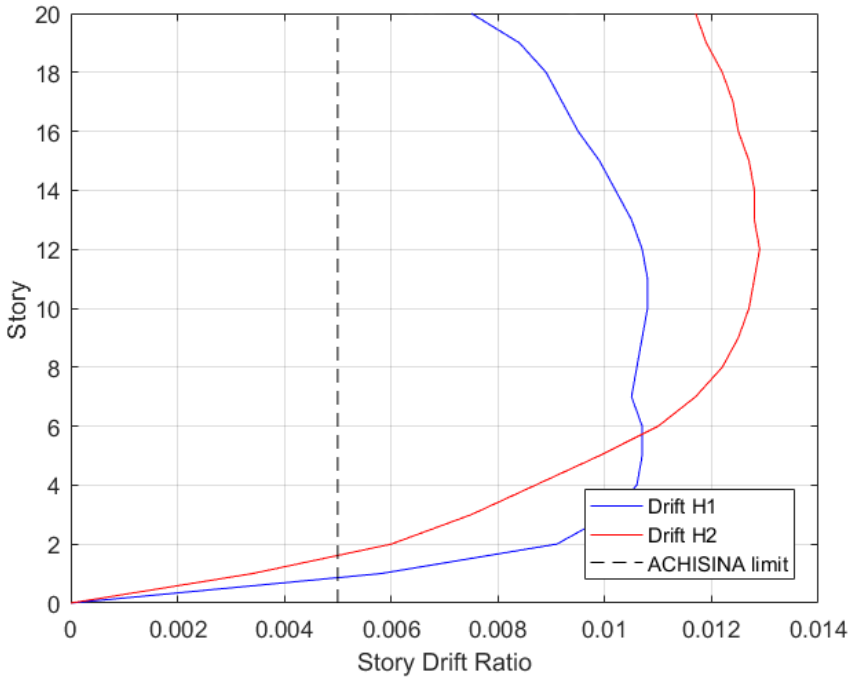

Fig. 5.15. Maximum story drifts at each story level for the model with slabs.

After working with the original model from Chapter 4 and the two alternative approaches presented in this subchapter, the local criteria presented different results, mostly with problems with the strain distribution in walls for the expected performance objectives. However, for the global acceptance criteria, all models exceeded the 0.005 story drift limit established by ACHISINA for the SD.

The following subchapter will present a comparative analysis between the ACHISINA and the LATBSDC (2015) procedures to review the analysis and design methodologies, compare performance objectives for different earthquakes, and conclude.

5.5 Comparison between ACHISINA and LATBSDC requirements

The ACHISINA procedure was based mainly on the Los Angeles Tall Building Structural Design Council procedure (LATBSDC, 2015), which defines two earthquakes for the performance-based design of tall buildings: the Service Level Earthquake (SLE) and the Maximum Considered Earthquake (MCE_R). In addition, the definition of materials, structural

actions (force-controlled and deformation-controlled), and the mathematical model are similar to the ACHISINA procedure for reinforced concrete shear walls.

The LATBSDC procedure defines the MCE_R as an earthquake for which the building has a low probability of collapse, on the order of 10% or less, assuming standard structural fragility. The performance objective is Collapse Prevention, which differs from the additional deformation capacity objective defined by the ACHISINA document for the SMC and will not be approached in this subchapter.

The SLE is an earthquake having a return period of T_r = 43 years, that is, a 50% probability of exceedance in 30 years, obtaining a site-specific, linear, uniform hazard acceleration response spectrum considering a damping level that must not be greater than 5%. The serviceability evaluation accepts either linear response spectrum analyses for the 1.0 D + L_{exp} + 1.0 E_x + 0.3 E_y and 1.0 D + L_{exp} + 0.3 E_x + 1.0 E_y load combinations or non-linear dynamic response analysis for the 1.0 D + L_{exp} + 1.0 E combination, similar to the ACHISINA document for both ground motions.

An Immediate Occupancy performance is expected for the SLE, meaning that the building's structural and non-structural elements remain serviceable after this event. For this seismic event, the limits for this case of study are the same as the ones presented in Table 4.1 for the SD, 0.005 limits for story drift, and the same local criteria for force and deformation-controlled elements.

The building studied in this research project is located in the hills of San Pedro de la Paz, Chile, funded on the soil type C (V_{s30} ranges between 404 m/s and 414 m/s) (FUCHIGE, 2014) and seismic zone 3 defined by NCh433. Fig. 5.16 shows the uniform hazard spectra (UHS) obtained with the R-CRISIS software (Ordaz & Salgado-Galvez, 2018), weighing results with five different GMPEs (Appendix B). UHS are compared with code-based spectra for the SD and the SMC levels.

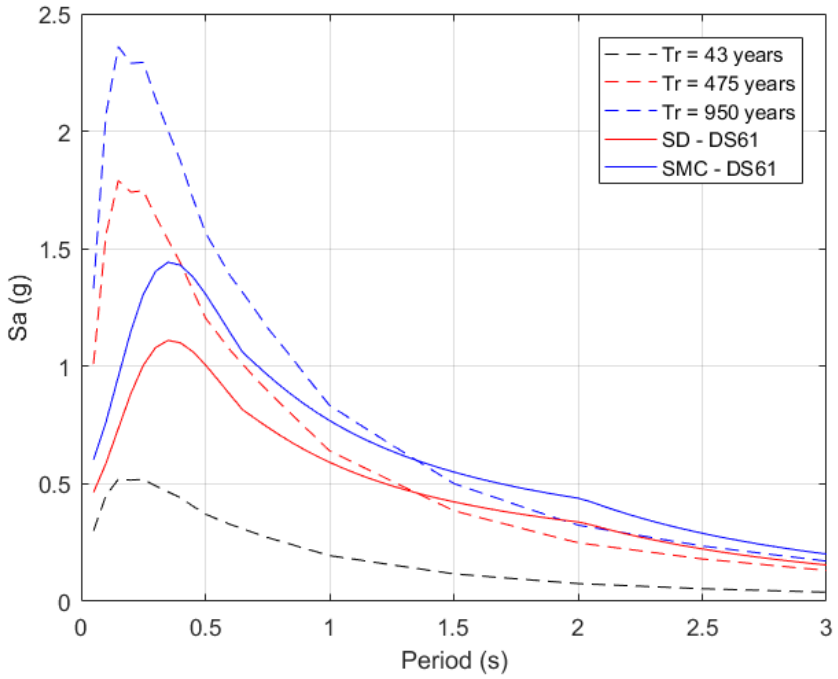

Fig. 5.16. Comparison between UHS for three different return periods and the code-based SD and SMC spectra.

The black, red, and blue dashed lines correspond to the SLE (defined only by LATBSDC), SD, and SMC design spectra, respectively, the last two defined with the return periods specified in the ACHISINA document. Compared with the code-based spectra (NCh433+DS61), the UHS spectra for the SD and SMC levels reach a peak 60% higher than those obtained from NCh433+DS61, and for periods higher than 1.35 s, the spectral acceleration values are below the NCH433+DS61 spectra.

As indicated before, ACHISINA limits for the SD level are the same established by LATBSDC for the SLE. Thus, for study purposes, the seismic performance of the analyzed building was now assessed through nonlinear dynamic analysis using five records compatible with the UHS spectrum with T_r=43 years obtained from PSHA. Fig. 5.17 presents the response spectra of the selected records for the SLE analysis after spectra matching.

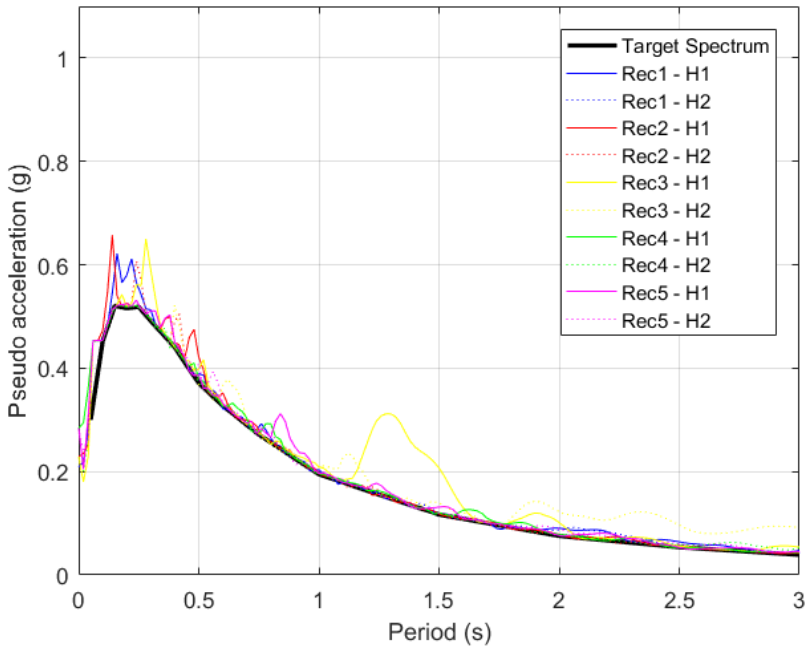

Fig. 5.17. Response spectra for the matched SLE earthquakes for nonlinear analysis.

Fig. 5.18. Fig. 5.19, and Table 5.7 show the strains, drifts, and shear results for these earthquakes, respectively. The building satisfies all SLE criteria, most importantly, drift results, which were the central issue in analyses presented in the last subchapter.

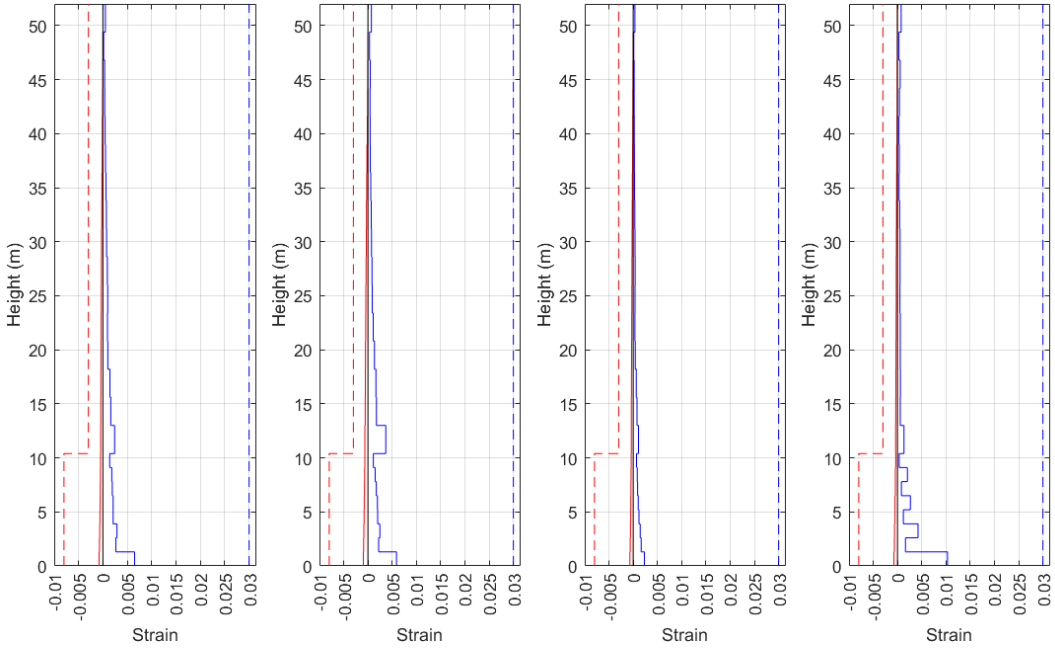

Fig. 5.18. SLE strain profiles for Walls 1, 2, 3, and 4 for the model with elastic slabs.

SLE (λ = 1.5)	Wall 1	Wall 2 (H_1)	Wall 2 (H_2)	Wall 3	Wall 4
Max λ V_u (ton)	289	328	387	125	1055
ϕ V_n (ton)	880	678	678	473	1490
λ V_u / ϕ V_n	0.33	0.49	0.57	0.26	0.71

Table 5.7. Maximum shear values obtained for the SLE earthquakes per wall group.

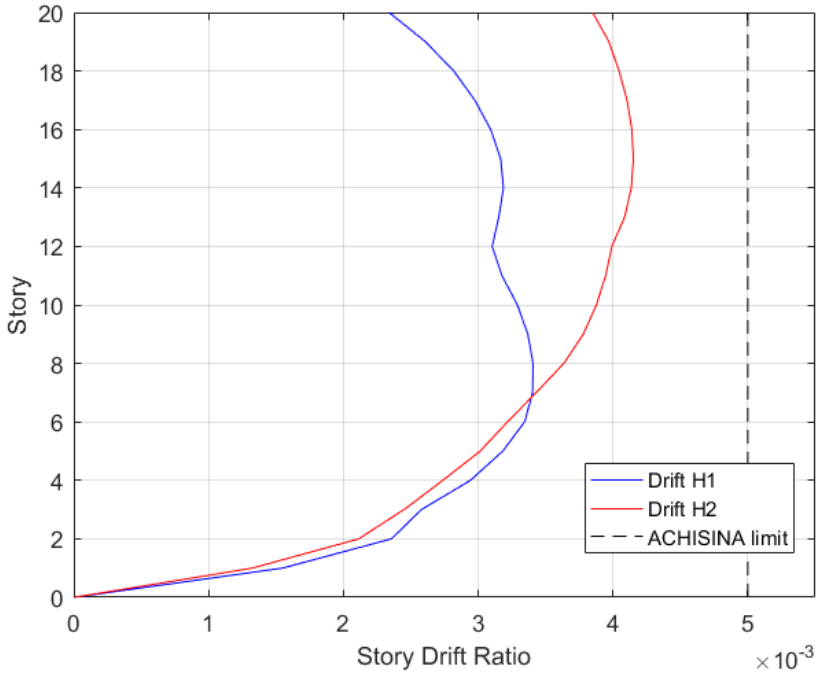

Fig. 5.19. Maximum story drifts for the SLE at each story level.

5.6 Conclusion

Application of nonlinear analyses to the building designed with the NCh433 code gave different results for the tensile and compressive strains, shears, and story drifts, variating the ground motions and aspects of the model. Results for all story drifts, the global acceptance criteria for the SD, exceeded the limit established by the document for all different models and earthquakes while obtaining different results for the local acceptance criteria. Furthermore, an SLE analysis showed satisfactory results in the same regard. These results point out to check the limit values for the ACHISINA recommendations, addressed in the final chapter of this report.

CHAPTER 6 CONCLUSIONS AND CLOSING REMARKS

From these analyses, the studied building did not satisfy the ACHISINA requirements for the SD level, especially the global acceptance criteria (story drift limits), to ensure the immediate occupancy performance following the SD level earthquake. The building model considered different modeling approaches to check the behavior of the parameters defined by ACHISINA: a model with and without slabs and records with and without spectral matching. The model without slabs, only considering rigid diaphragms at each story level, was considered first because of lesser computational demand, obtaining results that exceeded the story drifts limits while mainly showing problems in transverse direction walls 2 and 4. The model with slabs reduced these drift values; however, the coupling effect and the increase in stiffness affected the values of strains and shears for the local criteria.

However, the building did not satisfy the story drift requirements for all modeling approaches. Also, a comparative analysis was made between the ACHISINA (2017) and LATBSDC (2018) documents for the performance-based design of tall buildings, focusing on the SD (ACHISINA) and SLE (LATBSDC) ground motions of each procedure. Both earthquakes aimed for the Immediate Occupancy performance objective; however, the seismic demands from the SD earthquake far exceeded the SLE ones, shown by the UHS and return periods.

After checking the results for the SD and SLE story drifts versus the defined limits in each document, it is advisable to check the SD story drift limit values established by ACHISINA, considering that code-based designed buildings may not satisfy the immediate occupancy criteria. Therefore, this requirement may be over-conservative to be considered in actual designs. It is also advisable to pay attention to the stress and strain concentration observed in nonlinear analysis in stories where the confinement at wall boundaries suddenly changes from special to ordinary boundary elements. In this case, this stiffness change and the strain concentration resulted in the plastic hinge moving from the base of the building to the fourth story, which traduces to a decreased ductility of the structure due to lower total lateral

displacements at the top of the walls. An alternative design approach should be evaluated where sudden changes in confinement steel are avoided, preferring a design where the confinement requirements are slowly reduced in consecutive stories. Conservative design, for example, a building with a higher wall density, might go against the ACHISINA's design objective, which is to obtain more economic buildings with a good seismic performance.

Finally, more research is needed to include buildings with different typologies beyond shear wall buildings, such as those found in office buildings (core walls and perimeter frames), and different locations (different seismic zone/soil type), which could be used to refine the immediate performance criteria for the procedure. Moreover, it is recommended to include different stories and assess the effect of soil-structure interaction on seismic performance, which should affect the stiffness and seismic demands on the building.

BIBLIOGRAPHY

ACHISINA. (2017). *Diseño Sísmico Basado en Desempeño*. http://www.achisina.cl/index.php/publicaciones/manuales-guias

ACI Committee 318. (2014). Building Code Requirements for Structural Concrete. In *American Concrete Institute*.

Boore, D. M., Watson-Lamprey, J., & Abrahamson, N. A. (2006). Orientation-independent measures of ground motion. *Bulletin of the Seismological Society of America*, *96*(4 A), 1502–1511. https://doi.org/10.1785/0120050209

Cando, M. A., Hube, M. A., Parra, P. F., & Arteta, C. A. (2020). Effect of stiffness on the seismic performance of code-conforming reinforced concrete shear wall buildings. *Engineering Structures*, *219*(July 2019), 110724. https://doi.org/10.1016/j.engstruct.2020.110724

Castro, S., Benavente, R., Crempien de la Carrera, J., Candia, G., & de la Llera Martin, J. C. (2020). *SIBER-RISK Strong Motion Database*. https://doi.org/10.7764/datasetuc/ing-uc.1170836_1

Computers & Structures Inc. (2016a). *ETABS 2016 User's Guide*.

Computers & Structures Inc. (2016b). *PERFORM-3D nonlinear analysis and performance assessment for 3D structures*. https://doi.org/10.1016/B978-0-323-04579-7.00350-6

Computers & Structures Inc. (2017). *Getting started with SAP2000* (Vol. 2, Issue 2). https://doi.org/10.1093/combul/42.2.22

FUCHIGE. (2014). *Resumen Caracterización Geotécnica*.

Hognestad, E. (1951). A study of combined bending and axial load in reinforced concrete members. In *Bulletin Series No. 399*. University of Illinois Engineering Experimental Station.

INN. (2009). *Norma Chilena Oficial NCh1537Of.2009: Diseño estructural - Cargas permanentes y cargas de uso*.

INN. (2010). *Norma Chilena Oficial NCh3171: Diseño estructural - Disposiciones generales y combinaciones de cargas*. 17.

INN. (2012). *Norma Chilena Oficial NCh433: Diseño Sismico de Edificios* (p. 77).

LATBSDC. (2015). *An Alternative Procedure for Seismic Analysis and Design of Tall*

Buildings Located in the Los Angeles Region.

Lowes, L. N., Lehman, D. E., & Baker, C. (2016). Recommendations for Modeling the Nonlinear Response of Slender Reinforced Concrete Walls Using PERFORM-3D. *SEAOC Convention*, *December*, 1–18. https://doi.org/10.1093/cercor/bhs078

Massone, L. M., Bonelli, P., Lagos, R., Lüders, C., Moehle, J., & Wallace, J. W. (2012). Seismic design and construction practices for RC structural wall buildings. *Earthquake Spectra*, *28*(SUPPL.1). https://doi.org/10.1193/1.4000046

MINVU. (2011a). *DS 60-Requisitos de diseño y cálculo para el hormigón armado*. Ministerio de Vivienda y Urbanismo.

MINVU. (2011b). *DS61 - Diseño Sísmico de Edificios*. Ministerio de Vivienda y Urbanismo.

Moehle, J. (2003). *Seismic Design of Reinforced Concrete Buildings*. McGraw-Hill Education. https://doi.org/10.1201/9781420064988.fmatt

NEHRP. (2010). *ATC-94, "Recommendations for seismic design of reinforced concrete wall buildings based on studies of the 2010 Chile earthquake," Applied Technology Council, Redwood City, California, USA, 2014.*

Ordaz, M., & Salgado-Galvez, M. A. (2018). *R-CRISIS Validation and Verification Document Program for Probabilistic Seismic Hazard Analysis*.

PEER. (2014). PEER/ATC 72-1 - Modeling and acceptance criteria for seismic design and analysis of tall buildings. *Ground Motion Database*, 1. http://peer.berkeley.edu/peer_ground_motion_database

Pugh, J. S., Lowes, L. N., & Lehman, D. E. (2015). Nonlinear line-element modeling of flexural reinforced concrete walls. *Engineering Structures*, *104*, 174–192. https://doi.org/10.1016/j.engstruct.2015.08.037

Saatcioglu, M., & Razvi, S. (1992). Strength and ductility of laterally confined concrete. *Journal of Structural Engineering*, *118*(6), 1590–1607. https://doi.org/10.1002/suco.202000299

Seismosoft. (2022). *SeismoMatch 2022 – A computer program for spectrum matching of earthquake records* (p. available from http://seismosoft.com/).

Thomsen IV, J. H., & Wallace, J. W. (1995). *Displacement-Based Design of Reinforced Concrete Structural Walls: An Experimental Investigation of Walls with Rectangular and T-shaped Cross-Sections*.

Ugalde, D., Lopez-Garcia, D., & Parra, P. F. (2020). Fragility-based analysis of the influence of effective stiffness of reinforced concrete members in shear wall buildings. *Bulletin of Earthquake Engineering*, *18*(5), 2061–2082. https://doi.org/10.1007/s10518-020-00786-3

Ugalde, D., Parra, P. F., & Lopez-Garcia, D. (2019). Assessment of the seismic capacity of tall wall buildings using nonlinear finite element modeling. *Bulletin of Earthquake Engineering*, *17*(12), 6565–6589. https://doi.org/10.1007/s10518-019-00644-x

APPENDIX A CONCRETE CONSTITUTIVE CURVES

A1 Confined concrete strength

Eq. A-1 to Eq. A-5 define the confined concrete strength as proposed by Saatcioglu and Razvi (1992) for a square column

$$f'_{cc} = f'_{co} + k_1 f_{le} \quad \text{Eq. A-1}$$

$$f_{le} = k_2 f_l \quad \text{Eq. A-2}$$

$$f_l = \frac{\sum A_s f_{yt} \sin\alpha}{s b_c} \quad \text{Eq. A-3}$$

$$k_2 = 0.26\sqrt{\left(\frac{b_c}{s}\right)\left(\frac{b_c}{s_l}\right)\left(\frac{1}{f_l}\right)} \quad \text{Eq. A-4}$$

$$k_1 = 6.7\,(f_{le})^{-0.17} \quad \text{Eq. A-5}$$

where f'_{cc} and f'_{co} are the confined and unconfined concrete strength, f_{le} and f_l are the equivalent and average uniform lateral pressure in MPa units, k_1 and k_2 are coefficients that depend on these pressures.

For rectangular columns, the formulation is the same, taking the lateral pressure as

$$f_{le} = \frac{f_{le_x} b_{cx} + f_{le_y} b_{cy}}{b_{cx} + b_{cy}} \quad \text{Eq. A-6}$$

where f_{le_x} and f_{le_y} are the effective lateral pressures acting perpendicular to core dimensions b_{cx} and b_{cy} respectively.

Eq. A-1 to Eq. A-6 give the concrete strength in the boundary elements on all walls of the studied building, considering them as rectangular columns. For example, the Wall 1 boundary (shown in Fig. A.1) element calculations use expected properties instead of nominal ones. Considering nominal values as f'_c = 25 MPa, f_y = 420 MPa, ACHISINA (2017) gives the following recommendations for expected properties

$$f'_{co} = 1.3 f'_c = 32.5 \text{ MPa}$$

$$f_{yt} = 1.17 f_y = 491 \text{ MPa}$$

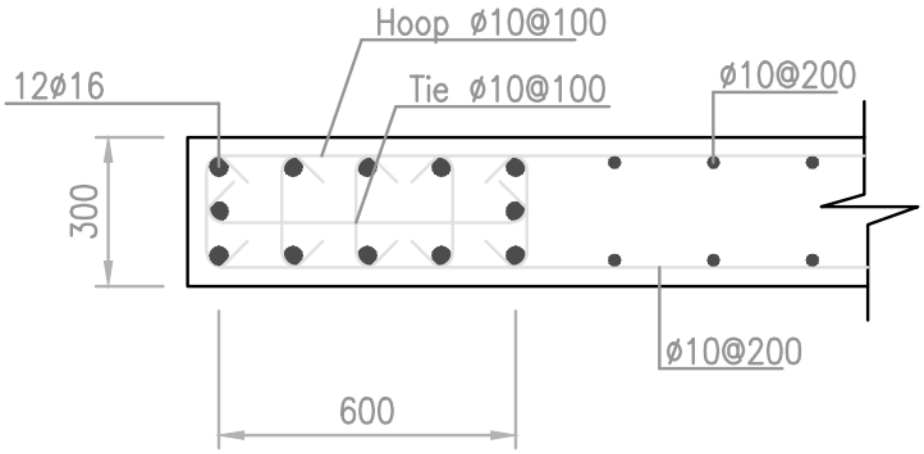

Fig. A.1. Wall 1 boundary element.

Then, Eq. A-2 to Eq. A-6 calculate the parameters for each direction of analysis, obtaining

$$k_1 = 6.4 \text{ (taking } f_l \text{ as } f_{l_{short}})$$

$$k_{2_{short}} = 0.3, \quad f_{l_{short}} = 4.4 \text{ MPa}, \quad f_{le_{short}} = 1.3 \text{ MPa}$$

$$k_{2_{long}} = 0.6, \quad f_{l_{long}} = 3.0 \text{ MPa}, \quad f_{le_{long}} = 1.9 \text{ MPa}$$

Distances $b_{c_{short}}$ and $b_{c_{long}}$ are the ones that define the core of the boundary element. In this case, assuming $b_{c_{short}} = 26\ cm$ and $b_{c_{long}} = 63.6\ cm$ and using Eq. A-6

$$f_{le} = \frac{f_{le_x} b_{cx} + f_{le_y} b_{cy}}{b_{cx} + b_{cy}} = 1.8 \text{ MPa}$$

Finally, Eq. A-1 calculates the strength of the confined concrete

$$f'_{cc_{W1}} = f'_{co} + k_1 f_{le} = 32.5 + 6.4 \cdot 1.8 = 43.7 \text{ MPa}$$

All boundary elements in all walls follow the same procedure, obtaining the following confined concrete strengths

$$f'_{cc_{W2_{flange}}} = 49.7 \text{ MPa}, \quad f'_{cc_{W2_{web}}} = 48.7 \text{ MPa}$$

$$f'_{cc_{W3}} = 45.7 \text{ MPa}, \quad f'_{cc_{W4}} = 47.9 \text{ MPa}$$

For simplicity in the modeling phase, the considered confined concrete strength was the minimum of all these values, $f'_{cc} = f'_{cc_{W1}} = 43.7$ MPa.

A2 Stress-strain relationship

The same document proposes a confined concrete stress-strain relationship based on the Hognestad (1951) model for unconfined concrete, consisting of a parabola for the ascending branch and a linear portion for the descending part. Fig. A.2 illustrates the proposed constitutive curves.

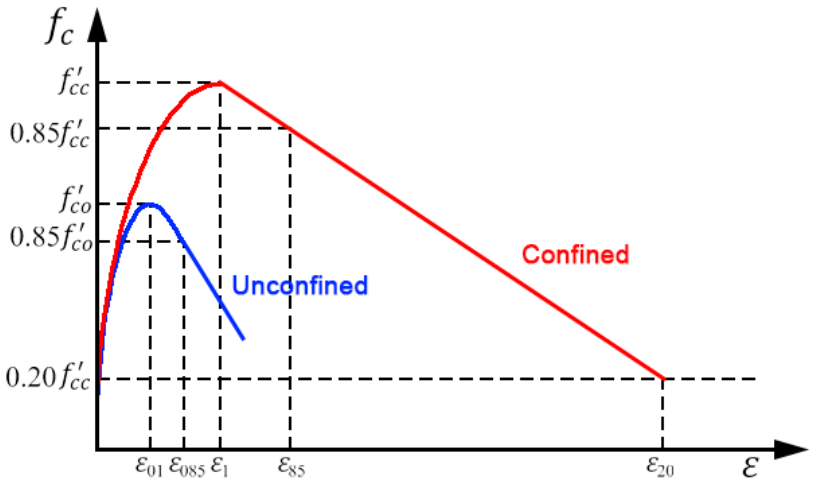

Fig. A.2. Proposed stress-strain relationship (adapted from Saatcioglu and Razvi, 1992).

For unconfined concrete, peak strain ε_{01} and strain at 85% strength level beyond the peak ε_{085} can be taken as 0.002 and 0.0038, respectively. For confined concrete, Eq. A-7 to Eq. A-10 give strains ε_1 and ε_{85}.

$$\varepsilon_1 = \varepsilon_{01}(1 + 5K) \quad \text{Eq. A-7}$$

$$K = \frac{k_1 f_{le}}{f'_{co}} \quad \text{Eq. A-8}$$

$$\varepsilon_{85} = 260\rho\varepsilon_1 + \varepsilon_{085} \quad \text{Eq. A-9}$$

$$\rho = \frac{\sum A_s}{s(b_{cx} + b_{cy})} \quad \text{Eq. A-10}$$

Eq. A-11 plots the parabolic portion of the curve for confined and unconfined concrete, while the linear part is obtained with the peak strain and the 85% strength level points, considering a constant residual strength at 20% strength level for confined concrete.

$$f_c = f'_{cc}\left[2\left(\frac{\varepsilon_c}{\varepsilon_1}\right) - \left(\frac{\varepsilon_c}{\varepsilon_1}\right)^2\right]^{\frac{1}{1+2K}} \leq f'_{cc} \qquad \text{Eq. A-11}$$

For simplicity, unconfined and confined concrete assumed a bi-linear constitutive curve, replacing the curved portion with a straight line, considering no residual strength for unconfined concrete. Fig. A.3 presents these curves for Wall 1 in MPa units.

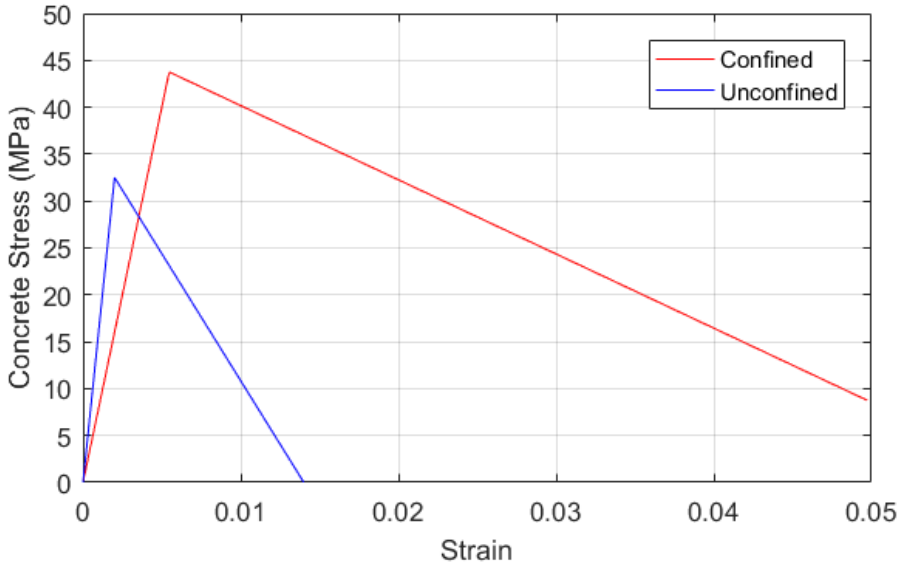

Fig. A.3. Proposed stress-strain relationship for Wall 1.

APPENDIX B SEISMIC HAZARD ANALYSIS RESULTS

The seismic hazard analysis used the commercial software R-CRISIS (Ordaz & Salgado-Galvez, 2018), considering the location in El Venado, Concepción, Chile (36°51'32" S, 73°05'35" O) and using five attenuation curves: Atkinson and Boore, Zhao *et al.*, Montalva *et al.*, Abrahamson *et al.* (BC Hydro), and Youngs *et al.* with the following weighting based on the location:

	Factor
Atkinson and Boore	0.05
Zhao	0.1
Montalva	0.5
BC Hydro	0.3
Youngs	0.05
	1

Table B.1. Weighting for the different attenuations for the PSHA.

This Appendix presents the tables for each UHS and average curve.

T(s)	**S_a (g) [Atkinson and Boore]**		
	T_r=43 yrs	**T_r=475 yrs**	**T_r=950 yrs**
0.05	0.473	1.730	2.290
0.10	0.576	2.360	3.200
0.15	0.589	2.370	3.190
0.20	0.603	2.380	3.180
0.25	0.598	2.320	3.100
0.30	0.593	2.280	3.030
0.35	0.588	2.230	2.960
0.40	0.584	2.180	2.880
0.45	0.558	2.100	2.790
0.50	0.531	2.020	2.680
0.55	0.505	1.930	2.570
0.60	0.477	1.840	2.460
0.65	0.450	1.750	2.340
0.70	0.422	1.650	2.220
0.75	0.393	1.550	2.090
0.80	0.365	1.450	1.950
0.85	0.335	1.340	1.810
0.90	0.306	1.230	1.660
0.95	0.276	1.110	1.510
1.00	0.246	0.991	1.350

T(s)	S_a (g) [Atkinson and Boore]		
	T_r=43 yrs	T_r=475 yrs	T_r=950 yrs
1.05	0.239	0.962	1.310
1.10	0.231	0.933	1.270
1.15	0.224	0.904	1.230
1.20	0.217	0.874	1.190
1.25	0.210	0.844	1.150
1.30	0.203	0.814	1.110
1.35	0.195	0.783	1.060
1.40	0.188	0.753	1.020
1.45	0.180	0.722	0.981
1.50	0.173	0.691	0.938
1.55	0.166	0.659	0.896
1.60	0.158	0.628	0.852
1.65	0.151	0.596	0.809
1.70	0.144	0.565	0.766
1.75	0.136	0.533	0.722
1.80	0.129	0.501	0.678
1.85	0.121	0.469	0.634
1.90	0.114	0.436	0.589
1.95	0.107	0.404	0.545
2.00	0.099	0.372	0.501
2.05	0.097	0.364	0.490
2.10	0.094	0.356	0.480
2.15	0.092	0.348	0.469
2.20	0.089	0.339	0.458
2.25	0.087	0.331	0.447
2.30	0.084	0.322	0.436
2.35	0.082	0.313	0.424
2.40	0.079	0.304	0.412
2.45	0.076	0.295	0.400
2.50	0.074	0.286	0.388
2.55	0.071	0.277	0.376
2.60	0.069	0.268	0.364
2.65	0.066	0.258	0.351
2.70	0.063	0.248	0.338
2.75	0.061	0.239	0.325
2.80	0.058	0.229	0.312
2.85	0.055	0.219	0.299
2.90	0.052	0.209	0.285
2.95	0.050	0.199	0.272
3.00	0.047	0.188	0.258

Table B.2. UHS results (Atkinson and Boore).

T(s)	S_a (g) [Zhao *et al.*]		
	T_r=43 yrs	T_r=475 yrs	T_r=950 yrs
0.05	0.325	1.110	1.460
0.10	0.548	1.920	2.560
0.15	0.725	2.540	3.390
0.20	0.754	2.610	3.460
0.25	0.714	2.450	3.250
0.30	0.659	2.260	2.980
0.35	0.569	1.930	2.550
0.40	0.480	1.620	2.120
0.45	0.430	1.440	1.890
0.50	0.382	1.270	1.660
0.55	0.344	1.140	1.500
0.60	0.305	1.010	1.330
0.65	0.286	0.960	1.260
0.70	0.267	0.905	1.190
0.75	0.252	0.864	1.130
0.80	0.238	0.822	1.080
0.85	0.228	0.788	1.040
0.90	0.218	0.755	0.993
0.95	0.209	0.727	0.957
1.00	0.200	0.700	0.921
1.05	0.193	0.679	0.895
1.10	0.186	0.657	0.867
1.15	0.178	0.636	0.840
1.20	0.171	0.614	0.813
1.25	0.164	0.592	0.785
1.30	0.157	0.573	0.760
1.35	0.152	0.553	0.734
1.40	0.145	0.533	0.708
1.45	0.139	0.514	0.682
1.50	0.133	0.494	0.656
1.55	0.129	0.480	0.638
1.60	0.125	0.466	0.620
1.65	0.121	0.452	0.601
1.70	0.118	0.438	0.583
1.75	0.114	0.424	0.564
1.80	0.110	0.410	0.546
1.85	0.106	0.396	0.527
1.90	0.102	0.382	0.508
1.95	0.098	0.367	0.489
2.00	0.094	0.353	0.471
2.05	0.092	0.344	0.459

T(s)	S_a (g) [Zhao *et al.*]		
	T_r=43 yrs	T_r=475 yrs	T_r=950 yrs
2.10	0.089	0.335	0.446
2.15	0.087	0.326	0.434
2.20	0.085	0.317	0.422
2.25	0.082	0.308	0.410
2.30	0.080	0.299	0.398
2.35	0.077	0.290	0.386
2.40	0.075	0.281	0.374
2.45	0.073	0.272	0.361
2.50	0.070	0.263	0.349
2.55	0.068	0.255	0.339
2.60	0.066	0.247	0.328
2.65	0.064	0.239	0.318
2.70	0.062	0.231	0.307
2.75	0.061	0.224	0.297
2.80	0.059	0.216	0.286
2.85	0.057	0.208	0.276
2.90	0.055	0.201	0.266
2.95	0.053	0.193	0.256
3.00	0.051	0.185	0.245

Table B.3. UHS results (Zhao *et al.*).

T(s)	S_a (g) [Montalva *et al.*]		
	T_r=43 yrs	T_r=475 yrs	T_r=950 yrs
0.05	0.364	1.240	1.640
0.10	0.548	1.900	2.530
0.15	0.624	2.140	2.840
0.20	0.600	2.010	2.650
0.25	0.620	2.080	2.730
0.30	0.578	1.900	2.480
0.35	0.547	1.770	2.300
0.40	0.517	1.640	2.130
0.45	0.469	1.480	1.910
0.50	0.424	1.320	1.710
0.55	0.397	1.240	1.600
0.60	0.371	1.160	1.490
0.65	0.349	1.080	1.400
0.70	0.325	1.010	1.310
0.75	0.302	0.938	1.210
0.80	0.283	0.874	1.130
0.85	0.264	0.811	1.050
0.90	0.244	0.747	0.963
0.95	0.225	0.684	0.881
1.00	0.205	0.621	0.799
1.05	0.196	0.593	0.762
1.10	0.188	0.565	0.725
1.15	0.179	0.536	0.688
1.20	0.170	0.509	0.652
1.25	0.161	0.481	0.616
1.30	0.153	0.453	0.580
1.35	0.144	0.426	0.545
1.40	0.135	0.399	0.510
1.45	0.127	0.372	0.475
1.50	0.118	0.345	0.440
1.55	0.113	0.331	0.422
1.60	0.109	0.317	0.404
1.65	0.104	0.303	0.386
1.70	0.100	0.290	0.369
1.75	0.095	0.276	0.351
1.80	0.090	0.263	0.334
1.85	0.086	0.249	0.317
1.90	0.081	0.236	0.300
1.95	0.077	0.223	0.284
2.00	0.073	0.211	0.268
2.05	0.070	0.203	0.259

T(s)	S_a (g) [Montalva *et al.*]		
	T_r=43 yrs	T_r=475 yrs	T_r=950 yrs
2.10	0.068	0.196	0.250
2.15	0.065	0.189	0.241
2.20	0.063	0.182	0.232
2.25	0.060	0.175	0.223
2.30	0.058	0.168	0.214
2.35	0.055	0.161	0.205
2.40	0.053	0.154	0.196
2.45	0.050	0.147	0.188
2.50	0.048	0.140	0.179
2.55	0.046	0.136	0.173
2.60	0.045	0.132	0.168
2.65	0.044	0.128	0.162
2.70	0.042	0.123	0.157
2.75	0.041	0.119	0.151
2.80	0.040	0.115	0.146
2.85	0.038	0.111	0.141
2.90	0.037	0.107	0.135
2.95	0.036	0.103	0.130
3.00	0.034	0.099	0.125

Table B.4. UHS results (Montalva *et al.*).

T(s)	S_a (g) [BC Hydro]		
	T_r=43 yrs	T_r=475 yrs	T_r=950 yrs
0.05	0.136	0.471	0.616
0.10	0.224	0.786	1.030
0.15	0.254	0.901	1.180
0.20	0.256	0.908	1.190
0.25	0.247	0.883	1.160
0.30	0.249	0.892	1.170
0.35	0.253	0.909	1.190
0.40	0.256	0.927	1.220
0.45	0.245	0.892	1.170
0.50	0.234	0.856	1.130
0.55	0.226	0.829	1.090
0.60	0.218	0.802	1.050
0.65	0.209	0.774	1.020
0.70	0.201	0.747	0.983
0.75	0.192	0.719	0.947
0.80	0.185	0.692	0.911
0.85	0.177	0.665	0.876
0.90	0.169	0.637	0.840
0.95	0.161	0.611	0.804
1.00	0.154	0.583	0.768
1.05	0.148	0.560	0.739
1.10	0.142	0.537	0.708
1.15	0.135	0.515	0.678
1.20	0.129	0.492	0.648
1.25	0.123	0.469	0.618
1.30	0.117	0.446	0.588
1.35	0.111	0.423	0.558
1.40	0.105	0.400	0.528
1.45	0.099	0.378	0.498
1.50	0.093	0.355	0.468
1.55	0.090	0.344	0.453
1.60	0.087	0.332	0.438
1.65	0.084	0.321	0.424
1.70	0.081	0.310	0.409
1.75	0.078	0.299	0.394
1.80	0.075	0.288	0.379
1.85	0.072	0.276	0.365
1.90	0.069	0.265	0.350
1.95	0.066	0.254	0.335
2.00	0.063	0.243	0.321
2.05	0.062	0.237	0.313

T(s)	S_a (g) [BC Hydro]		
	T_r=43 yrs	T_r=475 yrs	T_r=950 yrs
2.10	0.060	0.231	0.305
2.15	0.059	0.225	0.297
2.20	0.057	0.220	0.290
2.25	0.055	0.214	0.282
2.30	0.054	0.208	0.274
2.35	0.052	0.202	0.266
2.40	0.051	0.196	0.259
2.45	0.049	0.190	0.251
2.50	0.048	0.184	0.243
2.55	0.047	0.180	0.238
2.60	0.046	0.176	0.232
2.65	0.044	0.172	0.227
2.70	0.043	0.168	0.221
2.75	0.042	0.164	0.216
2.80	0.041	0.159	0.210
2.85	0.040	0.155	0.205
2.90	0.039	0.151	0.200
2.95	0.038	0.147	0.194
3.00	0.037	0.143	0.189

Table B.5. UHS results (BC Hydro).

T(s)	S_a (g) [Youngs *et al.*]		
	T_r=43 yrs	T_r=475 yrs	T_r=950 yrs
0.05	0.421	1.030	1.260
0.10	0.536	1.310	1.610
0.15	0.606	1.490	1.820
0.20	0.677	1.660	2.040
0.25	0.662	1.630	2.000
0.30	0.646	1.600	1.960
0.35	0.605	1.500	1.840
0.40	0.563	1.400	1.720
0.45	0.524	1.310	1.610
0.50	0.486	1.230	1.510
0.55	0.462	1.170	1.440
0.60	0.437	1.110	1.370
0.65	0.412	1.050	1.300
0.70	0.389	0.992	1.220
0.75	0.364	0.934	1.150
0.80	0.346	0.889	1.100
0.85	0.327	0.843	1.040
0.90	0.308	0.798	0.987
0.95	0.291	0.753	0.931
1.00	0.272	0.708	0.877
1.05	0.262	0.684	0.848
1.10	0.251	0.660	0.820
1.15	0.241	0.635	0.790
1.20	0.230	0.611	0.760
1.25	0.219	0.585	0.729
1.30	0.208	0.560	0.698
1.35	0.197	0.533	0.666
1.40	0.186	0.507	0.634
1.45	0.175	0.480	0.602
1.50	0.164	0.453	0.569
1.55	0.160	0.443	0.557
1.60	0.155	0.433	0.545
1.65	0.151	0.423	0.532
1.70	0.146	0.412	0.519
1.75	0.142	0.401	0.507
1.80	0.137	0.390	0.493
1.85	0.132	0.379	0.480
1.90	0.128	0.367	0.466
1.95	0.123	0.356	0.452
2.00	0.118	0.344	0.437
2.05	0.116	0.339	0.432

T(s)	S_a (g) [Youngs *et al.*]		
	T_r=43 yrs	T_r=475 yrs	T_r=950 yrs
2.10	0.114	0.334	0.426
2.15	0.112	0.329	0.420
2.20	0.109	0.324	0.414
2.25	0.107	0.319	0.408
2.30	0.105	0.314	0.402
2.35	0.103	0.308	0.395
2.40	0.100	0.303	0.388
2.45	0.098	0.297	0.382
2.50	0.096	0.291	0.374
2.55	0.093	0.285	0.367
2.60	0.091	0.279	0.360
2.65	0.088	0.273	0.352
2.70	0.086	0.267	0.344
2.75	0.083	0.260	0.336
2.80	0.081	0.253	0.328
2.85	0.078	0.246	0.320
2.90	0.075	0.239	0.311
2.95	0.073	0.232	0.302
3.00	0.070	0.225	0.293

Table B.6. UHS results (Youngs *et al.*).

T(s)	S_a (g) [Average]		
	T_r=43 yrs	T_r=475 yrs	T_r=950 yrs
0.05	0.300	1.010	1.328
0.10	0.452	1.561	2.071
0.15	0.520	1.787	2.364
0.20	0.516	1.740	2.289
0.25	0.519	1.747	2.293
0.30	0.492	1.638	2.139
0.35	0.466	1.537	2.002
0.40	0.441	1.439	1.873
0.45	0.405	1.322	1.715
0.50	0.371	1.206	1.570
0.55	0.349	1.138	1.478
0.60	0.327	1.069	1.385
0.65	0.309	1.008	1.314
0.70	0.290	0.952	1.241
0.75	0.272	0.895	1.164
0.80	0.256	0.844	1.099
0.85	0.241	0.793	1.034
0.90	0.225	0.742	0.965
0.95	0.210	0.691	0.899
1.00	0.195	0.640	0.833
1.05	0.187	0.615	0.800
1.10	0.179	0.589	0.766
1.15	0.171	0.563	0.732
1.20	0.163	0.538	0.699
1.25	0.155	0.512	0.666
1.30	0.148	0.486	0.633
1.35	0.140	0.461	0.600
1.40	0.132	0.436	0.567
1.45	0.125	0.411	0.534
1.50	0.117	0.386	0.501
1.55	0.113	0.372	0.483
1.60	0.109	0.358	0.465
1.65	0.104	0.344	0.447
1.70	0.100	0.331	0.430
1.75	0.096	0.317	0.412
1.80	0.092	0.303	0.394
1.85	0.088	0.289	0.376
1.90	0.084	0.276	0.359
1.95	0.080	0.262	0.341
2.00	0.076	0.250	0.324
2.05	0.073	0.242	0.315

T(s)	S_a (g) [Average]		
	T_r=43 yrs	T_r=475 yrs	T_r=950 yrs
2.10	0.071	0.235	0.306
2.15	0.069	0.228	0.297
2.20	0.067	0.222	0.289
2.25	0.065	0.215	0.280
2.30	0.062	0.208	0.271
2.35	0.060	0.201	0.262
2.40	0.058	0.194	0.253
2.45	0.056	0.187	0.245
2.50	0.054	0.180	0.235
2.55	0.052	0.176	0.229
2.60	0.051	0.171	0.223
2.65	0.049	0.166	0.216
2.70	0.048	0.161	0.210
2.75	0.046	0.156	0.203
2.80	0.045	0.151	0.197
2.85	0.043	0.146	0.191
2.90	0.042	0.141	0.184
2.95	0.040	0.136	0.178
3.00	0.039	0.131	0.171

Table B.7. UHS results (weighted average).